PHYSICAL REVIEW D **88,** 014019 (2013)

Impact of Z' and universal extra dimension parameters on different asymmetries in $B_s \to \phi \ell^+ \ell^-$ decays

Ishtiaq Ahmed,[1,2,*] M. Jamil Aslam,[1,2,†] and M. Ali Paracha[3,4,‡]

[1]*National Centre for Physics, Quaid-i-Azam University Campus, Islamabad 45320, Pakistan*
[2]*Department of Physics, Quaid-i-Azam University, Islamabad 45320, Pakistan*
[3]*Centre for Advanced Mathematics and Physics, National University of Science and Technology, Islamabad 44000, Pakistan*
[4]*Laboratorio de Física Teórica e Computação Cientfica, Universidade Cruzeiro do Sul, 01506-000 São Paulo, Brazil*

(Received 21 April 2013; published 15 July 2013)

A comprehensive study of the impact of new physics on different observables for $B_s \to \phi \ell^+ \ell^-$ is carried out. We examine the new physics models, such as Z' and universal extra dimension models, where the effects of new physics come through the modification of Wilson coefficients. We analyze these effects through the theoretical prediction of the branching ratio, the forward-backward asymmetry, lepton polarization asymmetries, and the helicity fractions of the final-state meson. These observables will definitely be measured in present and future colliders with great precision. We also point out that hadronic uncertainties in various physical observables are small, which make them an ideal probe to establish new physics. Therefore, the measurements of these observables for the same decay would permit the detection of physics beyond the Standard Model and will also help us to distinguish between different new physics scenarios.

DOI: 10.1103/PhysRevD.88.014019 PACS numbers: 13.20.He

I. INTRODUCTION

Studies of flavor-changing neutral current (FCNC) decays have played a pivotal role in formulating the theoretical description of particle physics known as the Standard Model (SM). In the SM, at tree level, all the neutral currents conserve flavor so that FCNC decays do not occur at lowest order and are induced by the Glahsow-Iliopoulos-Maiani amplitude [1] at the loop level, which make their effective strength small. In addition to this loop suppression these are also suppressed in the SM due to their dependence on the weak mixing angles of the Cabbibo-Kobayashi-Maskawa (CKM) matrix $V_{\rm CKM}$ [2,3]. Therefore, these two circumstances make the FCNC decays relatively rare and hence important to provide stringent tests of SM in the flavor sector.

Although many measurements of observables in the B-meson systems agree with the SM, there are several observables whose measured values differ from the predictions of the SM, such as the following. (i) The values of the $B_d^0 - \bar{B}_d^0$ mixing phase $\sin(2\beta)$ obtained from different penguin-dominated $b \to s$ channels tend to be systematically smaller than that obtained from $B_d^0 \to J/\psi K_s$ [4–6]. (ii) The $B_s^0 - \bar{B}_s^0$ mixing phase measured by the CDF and D0 collaboration deviates from the SM prediction [7,8]. (iii) In $B \to K\pi$ decays, it is difficult to account for all the experimental measurements within the SM [9]. (iv) The isospin asymmetry between the neutral and charged decay modes of the $\bar{B} \to \bar{K}^* \ell^+ \ell^-$ decay also deviates from the SM [10]. These disagreements are typically at the 2σ level—which are not statistically significant—but these are still fertile ground to test SM and check the new physics (NP), as they appear in the $b \to s$ transitions. In this context there have been numerous papers examining the possible NP FCNC scenarios through the various $b \to s$ processes [11].

On the experimental side, the LHC is already up and running—where CMS, ATLAS, and LHCb have started taking data—while the Belle II is on its way. We are already witnessing that the SM is still standing tall at least in the data taken to date, and the recent discovery of a Higgs-like boson in the mass range of 126 GeV has left enough breathing room for the SM. It is therefore an ideal time to test the predictions of the SM and try to identify the nature of the physics that is beyond it.

Moreover, in the SM the zero crossing of the leptons' forward-backward asymmetry $[A_{\rm FB}(q^2)]$ in $B \to K^* l^+ l^-$ is at a well-determined position which is free from the hadronic uncertainties at the leading order (LO) in strong coupling α_s [12–14]. On the other hand, the LHCb has announced the results of $A_{\rm FB}$, the fraction of longitudinal polarization F_L, and the differential branching ratio dB/dq^2 as a function of the dimuon invariant mass for the decay $\bar{B} \to \bar{K}^* \mu^+ \mu^-$ using 0.37 fb^{-1} of data taken in 2011 [15]. These results of $A_{\rm FB}(\bar{B} \to \bar{K}^* \mu^+ \mu^-)$ are close to the SM predictions with slight error bars, and thus they have overwritten the earlier measurements by *BABAR* and Belle which measured this asymmetry with the opposite sign and with better statistics [15–18]. The collaboration plans to continue to study the channel $\bar{B} \to \bar{K}^* \mu^+ \mu^-$ in finer detail, with more angular variables, and is expected to achieve a high sensitivity to any small deviation from the SM [15].

In order to incorporate the experimental predictions of different physical observables in $\bar{B} \to \bar{K}^* \mu^+ \mu^-$ this decay has been studied in SM and in a number of different NP

*ishtiaq@ncp.edu.pk
†jamil@phys.qau.edu.pk
‡ali@ncp.edu.pk

scenarios [19–39] where NP effects display themselves through modifications in the Wilson coefficients as well as through the new operators. Besides these models the general analysis of $\bar{B} \to \bar{K}^* \mu^+ \mu^-$ decay has also been performed which allows us to include all possible NP operators, such as vector-axial vector, scalar-pseudoscalar, and tensor-axial tensor [40].

Apart from the ordinary B-meson decays an interesting avenue for the NP is opened by the B_s-meson decays, where $B_s^0 - \bar{B}_s^0$ mixing is the exciting feature, which in the SM originates from the box topologies and hence is strongly suppressed. In the presence of NP, new particles could give rise to additional box topologies and these decays can occurs at the tree level. In this regard, the key channel to address this possibility is the $B_s^0 \to J/\Psi\phi$, where the pertinent feature is that its final state contains two vector mesons and thereby requires the time-dependent angular analysis of the $J/\Psi \to \mu^+ \mu^-$ and $\phi \to K^+ K^-$ decay products [41]. In addition, over the last couple of years, measurements of CP-violating asymmetries in ''tagged'' analysis (distinguishing between initially present B_s^0 or $\bar{B}^0{}_s$ mesons) of the $B_s^0 \to J/\Psi\phi$ channel at the Tevatron indicate possible NP effects in $B_s^0 - \bar{B}_s^0$ mixing [42–44]. These results are complemented by the measurement of the anomalous like-sign dimuon charge asymmetry at D0, which was found to differ by 3.9σ from the SM prediction [45]. However, in the summer of 2012 the LHCb collaboration also reported results that disfavor large NP effects [46]. Therefore, more data is needed to clarify the potential and status of NP.

Along the same lines, the exclusive $B_s \to \phi \ell^+ \ell^-$ has also become attractive since at quark level these decays are also induced by $b \to s \ell^+ \ell^-$, and could be measured at the running Tevatron, LHC, and future super B factories. Recently, the CDF collaboration observed $B_s \to \phi \mu^+ \mu^-$ with the branching ratio [40]

$$\mathrm{Br}(B_s \to \phi \mu^+ \mu^-) = [1.44 \pm 0.33(\mathrm{stat}) \pm 0.46(\mathrm{syst})] \times 10^{-6}. \quad (1)$$

On the theoretical side this exclusive process is well studied in the literature [47–51] with varying degrees of theoretical rigor and emphasis. In order to study different physical observables—such as the dilepton invariant mass spectrum, the forward-backward asymmetry, the helicity fractions of final-state mesons, and different lepton polarization asymmetries—the crucial ingredients are the form factors which need to be calculated using a nonperturbative QCD methods and therefore form the bulk of theoretical uncertainties. Form factors parametrizing $B_s \to \phi \mu^+ \mu^-$ have already been calculated in different models, such as light-cone sum rules (LCSRs) [52–54], the perturbative QCD approach [55], the relativistic constituent quark model [56], the constituent quark model [57], and the light-front quark model [58]. Among them, the LCSRs deal with form factors on the small-momentum region and are complementary to the lattice QCD approach and consistent with perturbative QCD, as well as with the heavy-quark limit; therefore, we will adopt the form factors calculated by this approach in our forthcoming analysis of $B_s \to \phi \ell^+ \ell^-$ decays in the SM and two different NP models, namely, Z' and universal extra dimensions (UED). The form factors calculated from LCSRs are restricted to the low-q^2 region, whereas in the high-q^2 region ongoing efforts aim at the first unquenched prediction from the lattice [59].

It is well known that the NP plays its role in the rare B-meson decays in two different ways: one is through the modification in the Wilson coefficients corresponding to the SM operators, and the other is due to the appearance of new operators in the effective Hamiltonian, which are absent in the SM. The UED and Z' models belong to the category commonly known as minimal flavor-violating models, which do not change the operator basis of the SM and hence their contribution is absorbed in the Wilson coefficients. In the present study, we perform an analysis of the branching ratio, the forward-backward asymmetry (A_{FB}), the helicity fraction of the final-state ϕ meson ($f_{L,T}$), and the lepton polarization asymmetries (both single and double) in the $B_s \to \phi \ell^+ \ell^-$ decay in the aforementioned NP scenarios.

The outline of the paper is as follows. In Sec. II we briefly discuss the different NP scenarios and introduce the effective Hamiltonian formalism for semileptonic rare B_s decays. Section III contains the definitions and parametrizations of $B_s \to \phi$ matrix elements and summarizes the form factor calculated in LCSRs. In Sec. IV, we display the mathematical expressions for the branching ratio, the forward-backward asymmetry, the helicity fractions of the ϕ meson, and the different lepton polarization asymmetries. Section V contains our numerical results for the above-mentioned physical observables in both the SM and in different NP scenarios where we show the influence of the NP parameters on the various asymmetries outlined above. A brief summary and some concluding remarks are also given at the end of this section.

II. THEORETIC AL FRAMEWORK

Calculating the decay amplitude of $B_s \to \phi \ell^+ \ell^-$ decays requires some theoretical steps. Among them the most important and relevant are

(i) the separation of short-distance effects (encoded in Wilson coefficients) from the long-distance QCD effects (encoded in the matrix elements) in the effective Hamiltonian, and

(ii) the calculation of matrix elements of local quark bilinear operators of the type $\langle \phi | J | B_s \rangle$ in terms of form factors.

As the effective Hamiltonian will be changed in different models we will therefore first describe the effective Hamiltonian in the aforementioned models, and postpone discussing the form factors until the next section.

A. Standard Model

At quark level the decay $B_s \to \phi\ell^+\ell^-$ is governed by the transition $b \to s\ell^+\ell^-$ for which the effective Hamiltonian can be written as

$$H_{\rm eff} = -\frac{4G_F}{\sqrt{2}} V_{tb}^* V_{ts} \sum_{i=1}^{10} C_i(\mu) O_i(\mu), \tag{2}$$

where $O_i(\mu)$ $(i = 1, \ldots, 6)$ are the four-quark operators, $i = 7, 8$ are dipole operators, and $i = 9, 10$ are the semileptonic operators. The $C_i(\mu)$ are the corresponding Wilson coefficients at the energy scale μ. The terms that correspond to the running of the u quark in the loop, i.e., $V_{ub}^* V_{us}$ can be safely ignored because $\frac{V_{ub}^* V_{us}}{V_{tb}^* V_{ts}} \prec 2 \times 10^{-2}$. The operators responsible for $B_s \to \phi\ell^+\ell^-$ are O_7, O_9, and O_{10} and their form is given by

$$\begin{aligned} O_7 &= \frac{e^2}{16\pi^2} m_b (\bar{s}\sigma_{\mu\nu} P_R b) F^{\mu\nu}, \\ O_9 &= \frac{e^2}{16\pi^2} (\bar{s}\gamma_\mu P_L b)(\bar{l}\gamma^\mu l), \\ O_{10} &= \frac{e^2}{16\pi^2} (\bar{s}\gamma_\mu P_L b)(\bar{l}\gamma^\mu \gamma_5 l), \end{aligned} \tag{3}$$

with $P_{L,R} = (1 \pm \gamma_5)/2$. The Wilson coefficients C_i can be calculated perturbatively and the explicit expressions of these in the SM at next-to-leading order and at next-to-next-to-leading logarithm are given in Refs. [60–75]. Since the Z boson is absent in the effective theory, the operator O_{10} cannot be induced by the insertion of four-quark operators. Hence, the Wilson coefficient C_{10} does not renormalize under QCD corrections and so it is independent of the energy scale.

The Wilson coefficient $C_9^{\rm SM}(\mu)$, which is commonly written as $C_9^{\rm eff}(\mu)$, corresponds to the semileptonic operator O_9. It can be decomposed into three parts,

$$C_9^{\rm SM} = C_9^{\rm eff}(\mu) = C_9(\mu) + Y_{\rm SD}(z, s') + Y_{\rm LD}(z, s'), \tag{4}$$

where the parameters z and s' are defined as $z = m_c/m_b$, $s' = q^2/m_b^2$. The short-distance function $Y_{\rm SD}(z, s')$ describes the perturbative part which includes the indirect contributions from the matrix element of four-quark operators $\sum_{i=1}^{6} \langle l^+ l^- s|O_i|b\rangle$ and this lies sufficiently far away from the $c\bar{c}$ resonance regions. The manifest expressions for $Y_{\rm SD}(z, s')$ can be written as [61,62]

$$\begin{aligned} Y_{\rm SD}(z, s') &= h(z, s')(3C_1(\mu) + C_2(\mu) + 3C_3(\mu) + C_4(\mu) \\ &\quad + 3C_5(\mu) + C_6(\mu)) - \frac{1}{2} h(1, s')(4C_3(\mu) \\ &\quad + 4C_4(\mu) + 3C_5(\mu) + C_6(\mu)) \\ &\quad - \frac{1}{2} h(0, s')(C_3(\mu) + 3C_4(\mu)) + \frac{2}{9}(3C_3(\mu) \\ &\quad + C_4(\mu) + 3C_5(\mu) + C_6(\mu)), \end{aligned} \tag{5}$$

with

$$\begin{aligned} h(z, s') &= -\frac{8}{9}\ln z + \frac{8}{27} + \frac{4}{9}x - \frac{2}{9}(2 + x)|1 - x|^{1/2} \begin{cases} \ln\left|\frac{\sqrt{1-x}+1}{\sqrt{1-x}-1}\right| - i\pi & \text{for } x \equiv 4z^2/s' < 1, \\ 2\arctan\frac{1}{\sqrt{x-1}} & \text{for } x \equiv 4z^2/s' > 1, \end{cases} \\ h(0, s') &= \frac{8}{27} - \frac{8}{9}\ln\frac{m_b}{\mu} - \frac{4}{9}\ln s' + \frac{4}{9} i\pi. \end{aligned} \tag{6}$$

The long-distance contributions $Y_{\rm LD}(z, s')$ from four-quark operators near the $c\bar{c}$ resonance cannot be calculated from the first principles of QCD and are usually parametrized in the form of a phenomenological Breit-Wigner formula, making use of the vacuum saturation approximation and quark-hadron duality. In the present study we ignore this part because this lies far away from the region of interest.

The nonfactorizable effects [76–78] from the charm loop can bring about further corrections to the radiative $b \to s\gamma$ transition, which can be absorbed into the effective Wilson coefficient $C_7^{\rm eff}$. Specifically, the Wilson coefficient $C_7^{\rm eff}$ is given by

$$C_7^{\rm SM} = C_7^{\rm eff}(\mu) = C_7(\mu) + C_{b\to s\gamma}(\mu), \tag{7}$$

with

$$C_{b\to s\gamma}(\mu) = i\alpha_s \left[\frac{2}{9}\eta^{14/23}(G_1(x_t) - 0.1687) - 0.03 C_2(\mu)\right], \tag{8}$$

$$G_1(x_t) = \frac{x_t(x_t^2 - 5x_t - 2)}{8(x_t - 1)^3} + \frac{3x_t^2 \ln^2 x_t}{4(x_t - 1)^4}, \tag{9}$$

where $\eta = \alpha_s(m_W)/\alpha_s(\mu)$, $x_t = m_t^2/m_W^2$, $C_{b\to s\gamma}$ is the absorptive part for the $b \to sc\bar{c} \to s\gamma$ rescattering, and we have dropped out the tiny contributions proportional to the CKM sector $V_{ub}V_{us}^*$.

In terms of the above Hamiltonian, the free quark decay amplitude for $b \to s\ell^+\ell^-$ in the SM can be derived as

$$\begin{aligned} \mathcal{M}(b \to s\ell^+\ell^-) &= -\frac{G_F \alpha}{\sqrt{2}\pi} V_{tb} V_{ts}^* \Big\{ C_9^{\rm SM}(\bar{s}\gamma_\mu P_L b)(\bar{l}\gamma^\mu l) \\ &\quad + C_{10}^{\rm SM}(\bar{s}\gamma_\mu P_L b)(\bar{l}\gamma^\mu \gamma_5 l) \\ &\quad - 2m_b C_7^{\rm SM}\left(\bar{s} i\sigma_{\mu\nu}\frac{q^\nu}{q^2} P_R b\right)(\bar{l}\gamma^\mu l)\Big\}, \end{aligned} \tag{10}$$

where $q^2 = (p_{l^+} + p_{l^-})^2$ is the square of the momentum transfer.

B. Universal extra dimension model

Among different new physics models proposed during the last 20 years or so, a special role is played by one with UED. In this model all SM fields are allowed to propagate in all available dimensions. The economy of the UED model is that there is only one additional parameter added to those of the SM—the radius R of the compactified extra dimension. Now above the compactification scale $1/R$ a given UED model becomes a higher-dimensional field theory whose equivalent description in four dimensions consists of SM fields and the towers of Kaluza-Klein (KK) modes having no partner in the SM. The simplest model of this type was proposed by Appelquist-Cheng-Dobrescu [79]. In this model, all the masses of the KK particles and their interactions with SM particles and also among themselves are described in terms of the inverse of the compactification radius R and the parameters of the SM [80,81].

The Appelquist-Cheng-Dobrescu model belongs to the class of minimal flavor-violating models where the effects beyond the SM are only encoded in the Wilson coefficients of the effective Hamiltonian without changing the operator basis of the SM. Wilson coefficients contributing in the calculation of $b \to s\ell^+\ell^-$, i.e., C_7, C_9, and C_{10} get modified due to the KK excitation, inducing a dependence on the compactification radius R. As the value of the compactification radius R becomes smaller—or in other words the value of $1/R$ becomes larger—we can recover the Standard Model phenomenology because the massive KK states start to decouple. As a general expression, the Wilson coefficients are represented by periodic functions $F(x_t, 1/R)$ generalizing their SM analogues $F_0(x_t)$,

$$F(x_t, 1/R) = F_0(x_t) + \sum_{n=1}^{\infty} F(x_t, x_n), \tag{11}$$

with $x_t = \frac{m_t^2}{M_w^2}$, $x_n = \frac{m_n^2}{M_w^2}$, and $m_n = \frac{n}{R}$. The remarkable feature of the above equation is that the summation over the KK contribution is finite at the leading order (LO) in all cases as a consequence of the generalized Glahsow-Iliopoulos-Maiani mechanism [80,81]. As $R \to 0$, $F(x_t, 1/R) \to F_0(x_t)$, which is the SM result. Now if we take $1/R$ to be a few hundred GeV, the values of the Wilson coefficients differ considerably from their corresponding SM values, where the most pronounced effects comes in the C_7. It is therefore expected that the various physical observables differ significantly from the SM results for a certain range of the compactification radius R.

Thus the effective Hamiltonian for $b \to s\ell^+\ell^-$ transition in a UED model is given by

$$\begin{aligned}\mathcal{H}_{\text{eff}}^{\text{UED}}(b \to s\ell^+\ell^-) &= -\frac{G_F\alpha}{\sqrt{2}\pi} V_{tb}V_{ts}^*\Big\{C_9^{\text{UED}}(\bar{s}\gamma_\mu P_L b)(\bar{l}\gamma^\mu l) \\ &+ C_{10}^{\text{UED}}(\bar{s}\gamma_\mu P_L b)(\bar{l}\gamma^\mu\gamma_5 l) \\ &- 2m_b C_7^{\text{UED}}\left(\bar{s}i\sigma_{\mu\nu}\frac{q^\nu}{q^2}P_R b\right)(\bar{l}\gamma^\mu l)\Big\},\end{aligned} \tag{12}$$

where the explicit expressions of various Wilson coefficients are given in Refs. [80,81]. Using this Hamiltonian the free quark decay amplitude becomes

$$\begin{aligned}\mathcal{M}(b \to s\ell^+\ell^-) &= -\frac{G_F\alpha}{\sqrt{2}\pi} V_{tb}V_{ts}^*\Big\{C_9^{\text{UED}}(\bar{s}\gamma_\mu P_L b)(\bar{l}\gamma^\mu l) \\ &+ C_{10}^{\text{UED}}(\bar{s}\gamma_\mu P_L b)(\bar{l}\gamma^\mu\gamma_5 l) \\ &- 2m_b C_7^{\text{UED}}\left(\bar{s}i\sigma_{\mu\nu}\frac{q^\nu}{q^2}P_R b\right)(\bar{l}\gamma^\mu l)\Big\}.\end{aligned} \tag{13}$$

C. Family nonuniversal Z' model

A family nonuniversal Z' boson could be derived naturally in many extensions of the SM, and the easiest way is to include an additional U′(1) gauge symmetry. This has been formulated in detail by Langacker and Plümacher [82]. Now in a family nonuniversal Z' model, FCNC transitions $b \to s\ell^+\ell^-$ could be induced at tree level because of the nondiagonal chiral coupling matrix. Taking for granted the fat that the couplings of right-handed quark flavors with the Z' boson are diagonal and ignoring $Z - Z'$ mixing, the effective Hamiltonian for $b \to s\ell^+\ell^-$ can be written as [83]

$$\begin{aligned}\mathcal{H}_{\text{eff}}^{Z'}(b \to s\ell^+\ell^-) &= -\frac{2G_F}{\sqrt{2}} V_{tb}^*V_{ts}B_{sb}\Big[\frac{4\pi}{\alpha V_{tb}^*V_{ts}}S_{\ell\ell}^L\bar{\ell}\gamma^\mu(1-\gamma^5)\ell \\ &- \frac{4\pi S_{\ell\ell}^R}{\alpha V_{tb}^*V_{ts}}\bar{\ell}\gamma^\mu(1+\gamma^5)\ell\Big]\bar{s}\gamma_\mu(1-\gamma^5)b + \text{H.c.},\end{aligned} \tag{14}$$

where $S_{\ell\ell}^L$ and $S_{\ell\ell}^R$ represent the coupling of the Z' boson with the left- and right-handed leptons, respectively, and B_{sb} corresponds to the of-diagonal left-handed coupling of quarks with the new Z' boson in a case when the weak phase ϕ_{sb} is neglected. In a situation when the weak phase is introduced in the off-diagonal coupling then this coupling reads as $B_{sb} = |B_{sb}|e^{-i\phi_{sb}}$. One can reformulate the effective Hamiltonian given in Eq. (14) as

$$\begin{aligned}H_{\text{eff}}^{Z'}(b \to s\ell^+\ell^-) &= -\frac{4G_F}{\sqrt{2}} V_{tb}^*V_{ts}[\bar{C}_9^{Z'}O_9 + \bar{C}_{10}^{Z'}O_{10}] + \text{H.c.},\end{aligned}$$

where

$$\bar{C}_9^{Z'} = \frac{4\pi e^{-i\phi_{sb}}}{\alpha V_{tb}^* V_{ts}} |B_{sb}| S_{LL}, \qquad \bar{C}_{10}^{Z'} = \frac{4\pi e^{-i\phi_{sb}}}{\alpha V_{tb}^* V_{ts}} |B_{sb}| D_{LL}, \tag{15}$$

with

$$S_{LL} = S_{\ell\ell}^L + S_{\ell\ell}^R, \qquad D_{LL} = S_{\ell\ell}^L - S_{\ell\ell}^R.$$

Hence the contribution of the Z' boson leads to the modification of the Wilson coefficients C_9 and C_{10}, which now take the form

$$C_9^{Z'} = C_9^{\rm SM} + \bar{C}_9^{Z'}, \qquad C_{10}^{Z'} = C_{10}^{\rm SM} + \bar{C}_{10}^{Z'},$$

while the Wilson coefficient C_7 remains unchanged.

III. MATRIX ELEMENTS AND FORM FACTORS IN LIGHT-CONE SUM RULES

In order to calculate the decay amplitudes for $B_s \to \phi \ell^+ \ell^-$ at hadron level, we have to sandwich the free quark amplitudes between the initial- and final-meson states. Consequently, the four hadronic matrix elements

$$\langle \phi(k,\varepsilon)|\bar{s}\gamma_\mu b|B_s(p)\rangle, \qquad \langle \phi(k,\varepsilon)|\bar{s}\gamma_\mu\gamma_5 b|B_s(p)\rangle,$$
$$\langle \phi(k,\varepsilon)|\bar{s}\sigma_{\mu\nu} b|B_s(p)\rangle, \qquad \langle \phi(k,\varepsilon)|\bar{s}\sigma_{\mu\nu}\gamma_5 b|B_s(p)\rangle \tag{16}$$

need to be computed. The above matrix elements can be parametrized in terms of the form factors as

$$\langle \phi(k,\varepsilon)|\bar{s}\gamma_\mu b|B_s(p)\rangle = \varepsilon_{\mu\nu\rho\sigma}\varepsilon^{*\nu} p^\rho k^\sigma \frac{2V(q^2)}{M_{B_s} + M_\phi}, \tag{17}$$

$$\begin{aligned}\langle \phi(k,\varepsilon)|\bar{s}\gamma_\mu\gamma_5 b|B_s(p)\rangle &= i\varepsilon_\mu^*(M_{B_s} + M_\phi)A_1(q^2) - i(p+k)_\mu(\varepsilon^*\cdot q) \\ &\times \frac{A_2(q^2)}{M_{B_s} + M_\phi} - iq_\mu(\varepsilon^*\cdot q)\frac{2M_\phi}{q^2}[A_3(q^2) - A_0(q^2)],\end{aligned} \tag{18}$$

$$\langle \phi(k,\varepsilon)|\bar{s}\sigma_{\mu\nu}q^\nu b|B_s(p)\rangle = i\varepsilon_{\mu\nu\rho\sigma}\varepsilon^{*\nu} p^\rho k^\sigma 2T_1(q^2), \tag{19}$$

$$\begin{aligned}\langle \phi(k,\varepsilon)|\bar{s}\sigma_{\mu\nu}\gamma_5 q^\nu b|B_s(p)\rangle &= T_2(q^2)[\varepsilon_\mu^*(M_{B_s}^2 - M_\phi^2) - (p+k)_\mu(\varepsilon^*\cdot q)] \\ &+ T_3(q^2)(\varepsilon^*\cdot q)\left[q_\mu - \frac{q^2}{M_{B_s}^2 - M_\phi^2}(p+k)_\mu\right],\end{aligned} \tag{20}$$

where all the form factors A_i and T_i are functions of the square of the momentum transfer $q^2 = (p-k)^2$ and $\varepsilon^{*\nu}$ is the polarization of the final-state vector meson (ϕ). The form factors A_i and T_i appearing in the above equations are not independent and can be related to one another with the help of equations of motion. The various relationships between the form factors are [51]

$$\begin{aligned}A_3(q^2) &= \frac{M_{B_s} + M_\phi}{2M_\phi}A_1(q^2) - \frac{M_{B_s} - M_\phi}{2M_\phi}A_2(q^2), \\ A_3(0) &= A_0(0), \qquad T_1(0) = T_2(0).\end{aligned} \tag{21}$$

The form factors for the $B_s \to \phi$ transition are the nonperturbative quantities and must be calculated using different approaches (both perturbative and nonperturbative), like lattice QCD, QCD sum rules, light-cone sum rules, etc. Here, we will consider the form factors calculated by using the light-cone sum rules approach by Ball and Braun [52]. The form factors V, A_0, and T_1 are parametrized by

$$F(q^2) = \frac{r_1}{1 - q^2/m_R^2} + \frac{r_2}{1 - q^2/m_{\rm fit}^2}, \tag{22}$$

while the form factors A_2 and $\tilde{T}_3$ are parametrized as

$$F(q^2) = \frac{r_1}{1 - q^2/m^2} + \frac{r_2}{(1 - q^2/m^2)^2}. \tag{23}$$

The fit formula for A_1 and T_2 is

$$F(q^2) = \frac{r_2}{1 - q^2/m_{\rm fit}^2}. \tag{24}$$

The form factor T_3 can be obtained through the relation

$$T_3(q^2) = \frac{M_{B_s}^2 - M_\phi^2}{q^2}[\tilde{T}_3(q^2 - T_2(q^2)],$$

where the values of different parameters are summarized in Table I.

From Eqs. (17)–(20) it is straightforward to find the matrix elements for $B_s \to \phi \ell^+ \ell^-$ as follows:

$$\begin{aligned}\mathcal{M} = -\frac{G_F\alpha}{2\sqrt{2}\pi M_{B_s}^2} V_{tb}V_{ts}^*[&\mathcal{T}_\mu^1(\bar{l}\gamma^\mu l) \\ &+ \mathcal{T}_\mu^2(\bar{l}\gamma^\mu\gamma_5 l) + \mathcal{T}^3(\bar{l}l)],\end{aligned} \tag{25}$$

where

TABLE I. Fit parameters for $B_s \to \phi$ transition form factors. $F(0)$ denotes the value of the form factors at $q^2 = 0$ [Eq. (22)] [52]. The theoretical uncertainty is estimated at around 15%.

$F(q^2)$	$F(0)$	r_1	m_R^2	r_2	$m_{\rm fit}^2$
$A_1(q^2)$	0.311	...	...	0.308	36.54
$A_2(q^2)$	0.234	−0.054	...	0.288	48.94
$A_0(q^2)$	0.474	3.310	5.28^2	−2.835	31.57
$V(q^2)$	0.434	1.484	5.32^2	−1.049	39.52
$T_1(q^2)$	0.349	1.303	5.32^2	−0.954	38.28
$T_2(q^2)$	0.349	...	...	0.349	37.21
$\tilde{T}_3(q^2)$	0.349	0.027	...	0.321	45.56

TABLE II. Wilson coefficients corresponding to the models discussed here.

	SM	UED	Z' model
$\tilde{C}_7$	$C_7^{\rm SM}$	$C_7^{\rm UED}$	$C_7^{\rm SM}$
$\tilde{C}_9$	$C_9^{\rm SM}$	$C_9^{\rm UED}$	$C_9^{Z'}$
$\tilde{C}_{10}$	$C_{10}^{\rm SM}$	$C_{10}^{\rm UED}$	$C_{10}^{Z'}$

$$\mathcal{T}^1_\mu = f_1(q^2)\epsilon_{\mu\nu\alpha\beta}\varepsilon^{*\nu}p^\alpha k^\beta - if_2(q^2)\varepsilon^*_\mu + if_3(q^2)(\varepsilon^*\cdot p)P_\mu, \tag{26}$$

$$\mathcal{T}^2_\mu = f_4(q^2)\epsilon_{\mu\nu\alpha\beta}\varepsilon^{*\nu}p^\alpha k^\beta - if_5(q^2)\varepsilon^*_\mu + if_6(q^2)(\varepsilon^*\cdot p)P_\mu + if_7(q^2)(\varepsilon^*\cdot p)P_\mu, \tag{27}$$

with $P_\mu = p_\mu + k_\mu$. The auxiliary functions appearing in the above equations can be written as

$$f_1(q^2) = 4\tilde{C}_7\left(\frac{m_b + m_s}{q^2}\right)T_1(q^2) + \tilde{C}_9\frac{2V(q^2)}{M_{B_s} + M_\phi}, \tag{28}$$

$$f_2(q^2) = 2\tilde{C}_7\left(\frac{m_b - m_s}{q^2}\right)T_2(q^2)(M^2_{B_s} - M^2_\phi) + \tilde{C}_9A_1(q^2)(M_{B_s} + M_\phi), \tag{29}$$

$$f_3(q^2) = 4\tilde{C}_7\left(\frac{m_b - m_s}{q^2}\right)\left(T_2(q^2) + q^2\frac{T_3(q^2)}{(M^2_{B_s} - M^2_\phi)}\right) + \tilde{C}_9\frac{A_+(q^2)}{M_{B_s} + M_\phi}, \tag{30}$$

$$f_4(q^2) = \tilde{C}_{10}\frac{2V(q^2)}{M_{B_s} + M_\phi}, \tag{31}$$

$$f_5(q^2) = 2\tilde{C}_{10}A_0(q^2)(M_{B_s} + M_\phi), \tag{32}$$

$$f_6(q^2) = 2\tilde{C}_{10}\frac{A_1(q^2)}{M_{B_s} + M_\phi}, \tag{33}$$

$$f_7(q^2) = 4\tilde{C}_{10}\frac{A_2(q^2)}{M_{B_s} + M_\phi}. \tag{34}$$

Here the Wilson coefficients $\tilde{C}_i$ will be different for different models, and these are gathered in Table II.

IV. FORMULA FOR OBSERVABLES

In this section we will present the calculations of the physical observables, such as the branching ratios $\mathcal{BR}$, the forward-backward asymmetries $\mathcal{A}_{\rm FB}$, the single lepton polarization asymmetries $P_{L,N,T}$, the double-lepton polarization asymmetries P_{ij} $(i, j = L, N, T)$, the helicity fractions $f_{L,T}$ of the ϕ meson, and the polarized and unpolarized CP asymmetries of the final-state lepton in $B_s \to \phi\ell^+\ell^-$ decay.

A. The differential decay rate

In the rest frame of the B_s meson the differential decay width of $B_s \to \phi\ell^+\ell^-$ can be written as

$$\frac{d\Gamma(B_s \to \phi\ell^+\ell^-)}{dq^2} = \frac{1}{(2\pi)^3}\frac{1}{32M^3_{B_s}}\int_{-u(q^2)}^{+u(q^2)} du|\mathcal{M}|^2, \tag{35}$$

where

$$q^2 = (p_+ + p_-)^2, \tag{36}$$

$$u = (p - p_-)^2 - (p - p_+)^2. \tag{37}$$

The limits on q^2 and u are

$$4m_l^2 \le q^2 \le (M_{B_s} - M_\phi)^2, \tag{38}$$

$$-u(q^2) \le u \le u(q^2), \tag{39}$$

with

$$u(q^2) = \sqrt{\lambda\left(1 - \frac{4m_l^2}{q^2}\right)} \tag{40}$$

and

$$\lambda \equiv \lambda(M^2_{B_s}, M^2_\phi, q^2) = M^4_{B_s} + M^4_\phi + q^4 - 2M^2_{B_s}M^2_\phi - 2M^2_\phi q^2 - 2q^2M^2_{B_s}. \tag{41}$$

In the above expressions, m_l corresponds to the mass of the lepton, which for our case can be μ or τ. The total decay rate for the decay $B_s \to \phi\ell^+\ell^-$ can take the form

$$\frac{d\Gamma}{dq^2} = \frac{G_F^2|V_{tb}V^*_{ts}|^2\alpha^2}{2^{11}\pi^5 3M^3_{B_s}M^2_\phi q^2}u(q^2)\times\mathcal{A}(q^2). \tag{42}$$

The function $u(q^2)$ is defined in Eq. (40) and $\mathcal{A}(q^2)$ is given by

$$\mathcal{A}(q^2) = 8M^2_\phi q^2\lambda\{(2m_l^2 + q^2)|f_1(q^2)|^2 - (4m_l^2 - q^2)|f_4(q^2)|^2\} + 4M^2_\phi q^2\{(2m_l^2 + q^2)(3|f_2(q^2)|^2 - \lambda|f_3(q^2)|^2) - (4m_l^2 - q^2)(3|f_5(q^2)|^2 - \lambda|f_6(q^2)|^2)\} + \lambda(2m_l^2 + q^2)|f_2(q^2) + (M^2_{B_s} - M^2_\phi - q^2)f_3(q^2)|^2 + 24m_l^2M^2_\phi\lambda|f_7(q^2)|^2 - (4m_l^2 - q^2)|f_5(q^2) + (M^2_{B_s} - M^2_\phi - q^2)f_6(q^2)|^2 - 12m_l^2q^2[\Re(f_5f_7^*) - \Re(f_6f_7^*)]. \tag{43}$$

B. Forward-backward asymmetries

The differential forward-backward asymmetry $\mathcal{A}_{\rm FB}$ of the final-state lepton can be written as

$$\frac{d\mathcal{A}_{\rm FB}(s)}{dq^2} = \int_0^1 \frac{d^2\Gamma}{dq^2 d\cos\theta} d\cos\theta - \int_{-1}^0 \frac{d^2\Gamma}{dq^2 d\cos\theta} d\cos\theta. \quad (44)$$

From an experimental point of view the normalized forward-backward asymmetry is more useful, which is defined as

$$\mathcal{A}_{\rm FB} = \frac{\int_0^1 \frac{d^2\Gamma}{dq^2 d\cos\theta} d\cos\theta - \int_{-1}^0 \frac{d^2\Gamma}{dq^2 d\cos\theta} d\cos\theta}{\int_{-1}^1 \frac{d^2\Gamma}{dq^2 d\cos\theta} d\cos\theta}.$$

The normalized $\mathcal{A}_{\rm FB}$ for $B_s \to \phi\ell^+\ell^-$ can be obtained from Eq. (35) as

$$\mathcal{A}_{\rm FB} = -\frac{1}{d\Gamma/dq^2} \frac{G_F^2\alpha^2}{2^{11}\pi^5 M_{B_s}^3} |V_{tb}V_{ts}^*|^2 q^2 u(q^2) \times \{4\,{\rm Re}[f_2^* f_4 + f_1^* f_5]\}, \quad (45)$$

where $d\Gamma/dq^2$ is given in Eq. (42). Confining ourselves to the SM, the above expression of the FB asymmetry in terms of the Wilson coefficients becomes

$$\mathcal{A}_{\rm FB} = -\frac{1}{d\Gamma/dq^2} \frac{G_F^2\alpha^2}{2^8\pi^5 M_{B_s}^3} |V_{tb}V_{ts}^*|^2 q^2 u(q^2) \times C_{10}\Big\{\Re(C_9^{\rm eff})V(q^2)A_1(q^2)\frac{m_b}{q^2}C_7^{\rm eff}(V(q^2)T_2(q^2) \times (M_{B_s} - M_\phi) + A_1(q^2)T_1(q^2)(M_{B_s} + M_\phi))\Big\}, \quad (46)$$

which is in agreement with the one obtained for $B \to K^* l^+ l^-$ decay in Ref. [13].

C. Lepton polarization asymmetries

In the rest frame of the lepton ℓ^-, the unit vectors along the longitudinal, normal, and transversal components of the ℓ^- can be defined as, respectively, [84–86],

$$s_{\rm L}^{-\mu} = (0, \vec{e}_{\rm L}^{-}) = \left(0, \frac{\vec{p}_-}{|\vec{p}_-|}\right), \quad (47a)$$

$$s_{\rm N}^{-\mu} = (0, \vec{e}_{\rm N}^{-}) = \left(0, \frac{\vec{k}\times\vec{p}_-}{|\vec{k}\times\vec{p}_-|}\right), \quad (47b)$$

$$s_{\rm T}^{-\mu} = (0, \vec{e}_{\rm T}^{-}) = (0, \vec{e}_{\rm N}\times\vec{e}_{\rm L}), \quad (47c)$$

where $\vec{p}_-$ and $\vec{k}$ are the three-momenta of the lepton ℓ^- and ϕ meson, respectively, in the c.m. frame of the $\ell^+\ell^-$ system. A Lorentz transformation is used to boost the longitudinal component of the lepton polarization to the c.m. frame of the lepton pair as

$$(s_{\rm L}^{-\mu})_{\rm c.m.} = \left(\frac{|\vec{p}_-|}{m_l}, \frac{E\vec{p}_-}{m_l|\vec{p}_-|}\right), \quad (48)$$

where E and m_l are the energy and mass of the lepton. The normal and transverse components remain unchanged under the Lorentz boost. The longitudinal ($P_{\rm L}$), normal ($P_{\rm N}$) and transverse ($P_{\rm T}$) polarizations of the lepton can be defined as

$$P_i^{(\mp)}(q^2) = \frac{\frac{d\Gamma}{dq^2}(\vec{\xi}^{\mp} = \vec{e}_i^{\,\mp}) - \frac{d\Gamma}{dq^2}(\vec{\xi}^{\mp} = -\vec{e}_i^{\,\mp})}{\frac{d\Gamma}{dq^2}(\vec{\xi}^{\mp} = \vec{e}_i^{\,\mp}) + \frac{d\Gamma}{dq^2}(\vec{\xi}^{\mp} = -\vec{e}_i^{\,\mp})}, \quad (49)$$

where $i = {\rm L}, {\rm N}, {\rm T}$ and $\vec{\xi}^{\mp}$ is the spin direction along the leptons $\ell^{\mp}$. The differential decay rate for the polarized lepton $\ell^{\mp}$ in $B_s \to \phi\ell^+\ell^-$ decay along any spin direction $\vec{\xi}^{\mp}$ is related to the unpolarized decay rate (42) by the following relation:

$$\frac{d\Gamma(\vec{\xi}^{\mp})}{dq^2} = \frac{1}{2}\left(\frac{d\Gamma}{dq^2}\right)[1 + (P_{\rm L}^{\mp}\vec{e}_{\rm L}^{\mp} + P_{\rm N}^{\mp}\vec{e}_{\rm N}^{\mp} + P_{\rm T}^{\mp}\vec{e}_{\rm T}^{\mp})\cdot\vec{\xi}^{\mp}]. \quad (50)$$

The expressions for the longitudinal, normal, and transverse lepton polarizations can be written as

$$P_{\rm L}(q^2) \propto \frac{4\lambda}{3M_\phi^2}\sqrt{\frac{q^2-4m_l^2}{q^2}} \times \Big\{2\Re(f_2 f_5^*) + \lambda\Re(f_3 f_6^*) + 4\sqrt{q^2}\Re(f_1 f_4^*)\left(1 + \frac{12q^2M_\phi^2}{\lambda}\right) + (-M_{B_s}^2 + M_\phi^2 + q^2)[\Re(f_3 f_5^*) + \Re(f_2 f_6^*)]\Big\}, \quad (51)$$

$$P_{\rm N}(q^2) \propto -\frac{m_l\pi}{M_\phi^2}\sqrt{\frac{\lambda}{q^2}} \times \{\lambda q^2\Re(f_3 f_7^*) - \lambda(M_{B_s}^2 - M_\phi^2)\Re(f_3 f_6^*) + \lambda\Re(f_3 f_5^*) + (M_{B_s}^2 - M_\phi^2 - q^2)[q^2\Re(f_2 f_7^*) + (M_{B_s}^2 - M_\phi^2)\Re(f_2 f_5^*)] + 8q^2M_\phi^2\Re(f_1 f_2^*)\}, \quad (52)$$

$$P_{\rm T}(q^2) \propto i\frac{m_l\pi\sqrt{\left(q^2 - \frac{4m_l^2}{q^2}\right)\lambda}}{M_\phi^2}\{M_\phi[4\Im(f_2 f_4^*) + 4\Im(f_1 f_5^*) + 3\Im(f_5 f_6^*)] - \lambda\Im(f_6 f_7^*) + (-M_{B_s}^2 + M_\phi^2 + q^2)\Im(f_7 f_5^*) - q^2\Im(f_5 f_6^*)\}, \quad (53)$$

where $f_1, f_2, \ldots, f_7$ are the auxiliary functions defined above. Here we have dropped the constant factors.

$$\Lambda_1 = \frac{1}{2}(1 + \gamma_5 \not{s}_i^-), \qquad \Lambda_2 = \frac{1}{2}(1 + \gamma_5 \not{s}_i^+), \quad (54)$$

D. Double-lepton polarization asymmetries

To calculate the double-polarization asymmetries, we consider the polarizations of both the lepton and antilepton simultaneously and introduce the following spin projection operators for the lepton ℓ^- and the antilepton ℓ^+ [87]:

where $i = \mathrm{L}$, T, and N correspond to the longitudinal, transverse, and normal lepton polarizations, respectively. In the rest frame of the lepton-antilepton one can define the following set of orthogonal vectors s^μ:

$$\begin{aligned} s_{\mathrm{L}}^{-\mu} &= (0, \vec{e}_{\mathrm{L}}^-) = \left(0, \frac{\vec{p}_-}{|\vec{p}_-|}\right), \qquad s_{\mathrm{N}}^{-\mu} = (0, \vec{e}_{\mathrm{N}}^-) = \left(0, \frac{\vec{k} \times \vec{p}_-}{|\vec{k} \times \vec{p}_-|}\right), \qquad s_{\mathrm{T}}^{-\mu} = (0, \vec{e}_{\mathrm{T}}^-) = (0, \vec{e}_{\mathrm{N}} \times \vec{e}_{\mathrm{L}}), \\ s_{\mathrm{L}}^{+\mu} &= (0, \vec{e}_{\mathrm{L}}^+) = \left(0, \frac{\vec{p}_+}{|\vec{p}_+|}\right), \qquad s_{\mathrm{N}}^{+\mu} = (0, \vec{e}_{\mathrm{N}}^+) = \left(0, \frac{\vec{k} \times \vec{p}_+}{|\vec{k} \times \vec{p}_+|}\right), \qquad s_{\mathrm{T}}^{+\mu} = (0, \vec{e}_{\mathrm{T}}^+) = (0, \vec{e}_{\mathrm{N}} \times \vec{e}_{\mathrm{L}}). \end{aligned} \quad (55)$$

Just as with the single-lepton polarization, through Lorentz transformations we can boost the longitudinal component of $\ell^-\ell^+$ in the c.m. frame as

$$(s_{\mathrm{L}}^{-\mu})_{\mathrm{c.m.}} = \left(\frac{|\vec{p}_-|}{m_l}, \frac{E\vec{p}_-}{m_l|\vec{p}_-|}\right) \qquad (s_{\mathrm{L}}^{+\mu})_{\mathrm{c.m.}} = \left(\frac{|\vec{p}_+|}{m_l}, -\frac{E\vec{p}_+}{m_l|\vec{p}_+|}\right) \quad (56)$$

The normal and transverse components remain the same under the Lorentz boost. We now define the double-lepton polarization asymmetries as

$$P_{ij}(q^2) = \frac{(\frac{d\Gamma}{dq^2}(\vec{s}_i^-, \vec{s}_i^+) - \frac{d\Gamma}{dq^2}(-\vec{s}_i^-, \vec{s}_i^+)) - (\frac{d\Gamma}{dq^2}(\vec{s}_i^-, -\vec{s}_i^+) - \frac{d\Gamma}{dq^2}(-\vec{s}_i^-, -\vec{s}_i^+))}{(\frac{d\Gamma}{dq^2}(\vec{s}_i^-, \vec{s}_i^+) - \frac{d\Gamma}{dq^2}(-\vec{s}_i^-, \vec{s}_i^+)) + (\frac{d\Gamma}{dq^2}(\vec{s}_i^-, -\vec{s}_i^+) - \frac{d\Gamma}{dq^2}(-\vec{s}_i^-, -\vec{s}_i^+))}, \quad (57)$$

where the subscripts i and j correspond to the lepton and antilepton polarizations, respectively. Using these definitions the various double-lepton polarization asymmetries as a function of q^2 can be written as

$$\begin{aligned} P_{\mathrm{LL}}(q^2) \propto \frac{1}{3m_l^2}\Big\{ & 4|f_1|^2(8m_l^4\lambda - q^2\mathcal{U}_2) + 4|f_4|^2\mathcal{U}_1 + \frac{1}{M_\phi^2}\Big[24m_l^4\lambda(M_{B_s}^2 - M_\phi^2)(f_6f_7^* + f_7f_6^*) - 12m_l^4\lambda(2f_5f_7^* + 2f_7f_5^*) \\ & + 12|f_7|^2m_l^4q^2\lambda + \Big((q^2 - M_{B_s}^2 + M_\phi^2)\Big(\frac{4m_l^4\lambda}{q^2} - 6m_l^2\lambda + \mathcal{U}_2\Big)\Big)(f_1f_2^* + f_2f_1^*) \\ & + |f_2|^2\Big(\frac{4m_l^4\lambda}{q^2}(\lambda + 12M_\phi^2q^2) - 3m_l^2(2\lambda + 8M_\phi^2q^2) + \mathcal{U}_2\Big) - \frac{4m_l^4}{q^2}\mathcal{U}_3(f_5^*f_6 + f_6^*f_5) \\ & + \lambda|f_6|^2\Big(\frac{4m_l^4}{q^2}\mathcal{U}_4 + 2m_l^2\lambda + \mathcal{U}_2\Big) + \lambda|f_5|^2\Big(\frac{4m_l^4}{q^2}(6(q^2 - M_{B_s}^2 + M_\phi^2)^2 - \lambda) - 3m_l^2(6\lambda + 8M_\phi^2q^2) + q^2\mathcal{U}_2\Big)\Big]\Big\}, \end{aligned} \quad (58)$$

$$\begin{aligned} P_{\mathrm{LT}} \propto \frac{1}{4M_\phi^2q^2}\pi\sqrt{\lambda}\sqrt{q^2 - 4m_l^2}\{ & 8m_lM_\phi^2q^2(f_2^*f_4 + f_2f_4^*) + 2m_l(M_{B_s}^2q^2(f_5^*f_7 + 3f_5^*f_6) + M_\phi^2q^2(4f_5^*f_1 - f_5^*f_7) \\ & - q^4(f_5^*f_7 + f_5^*f_6) - 2f_5^*f_6(M_{B_s}^2 - M_\phi^2)^2 + 2(M_{B_s}^2 - M_\phi^2)(|f_5|^2 - f_5f_6^*(M_{B_s}^2 - M_\phi^2)) + q^2(f_5f_6^*(3M_{B_s}^2 + M_\phi^2) \\ & - 2|f_5|^2) - f_5f_6^*q^4) + 4m_l\lambda(q^2(f_7f_6^* + f_6f_7^*) + |f_6|^2(M_{B_s}^2 - M_\phi^2))\}, \end{aligned} \quad (59)$$

$$\begin{aligned} P_{\mathrm{LN}} \propto -i\frac{1}{4M_\phi^2\sqrt{q^2}}\pi\sqrt{\lambda}\{ & 2m_l(M_B^2 - M_\phi^2 - q^2)(q^2f_2^*f_7 + f_2^*f_6(M_B^2 - M_\phi^2) - f_2^*f_5) \\ & + 2m_l\lambda(f_3^*f_5 - f_3^*f_6(M_B^2 - M_\phi^2) - q^2f_3^*f_7)\}, \end{aligned} \quad (60)$$

$$P_{\rm TL} \propto \frac{1}{4M_\phi^2 q^2}\pi\sqrt{\lambda}\sqrt{q^2-4m_l^2}\Big\{4m_l\lambda(q^2(f_6^*f_7+f_7^*f_6)+|f_7|^2(M_{B_s}^2-M_\phi^2))$$
$$-8m_lM_\phi^2q^2(f_4^*f_2+f_2^*f_4)+2m_l(q^2(M_\phi^2-M_{B_s}^2)f_5^*f_7+q^2(M_\phi^2+3M_{B_s}^2)f_5^*f_6+q^4(f_5^*f_7-f_5^*f_6)$$
$$-2f_5^*f_6(M_{B_s}^2-M_\phi^2)^2+q^2f_5^*f_6(3M_{B_s}^2+M_\phi^2)+2q^2f_5^*f_7(M_\phi^2-M_{B_s}^2)-2q^2|f_5|^2+q^4(2f_5f_7^*-f_5f_6^*)$$
$$+2(M_{B_s}^2-M_\phi^2)(|f_5|^2+f_5f_6^*(M_\phi^2-M_{B_s}^2))-4M_\phi^2q^2f_1f_5^*\Big(2\pi m_l\sqrt{\lambda}\sqrt{q^2-4m_l^2}\Big)\Big\}, \quad (61)$$

$$P_{\rm TN} \propto i\Big\{\frac{4}{3}q\sqrt{q^2-4m_l^2}(4\lambda-3M_{B_s}^4+6M_B^2(M_\phi^2+q^2)-3(M_\phi^2-q^2)^2)+\sqrt{q^2\lambda}u(f_1f_4^*+f_1^*f_4)\Big\}, \quad (62)$$

$$P_{\rm TT} \propto \frac{1}{3M_\phi^2q^2}\{48|f_2|^2m_l^2M_\phi^2q^2-4m_l^2(5|f_5|^2+(M_{B_s}^2-M_\phi^2)(f_3f_2^*-5f_5^*f_6))+(2|f_5|^2+12f_5f_7^*m_l^2$$
$$+(M_{B_s}^2-M_\phi^2)(f_3f_2^*-f_6f_5^*))+4m_l^2(3+f_3f_2^*+8M_\phi^2(|f_1|^2+|f_4|^2)-2f_6f_5^*)-2(3(M_{B_s}^2-M_\phi^2)f_6f_7^*$$
$$+3(M_{B_s}^2+M_\phi^2)|f_6|^2)+6q^2(f_7f_5^*-2f_7f_6^*(M_{B_s}^2-M_\phi^2))+2q^4(f_6f_5^*-f_3f_2^*+6m_l^2(|f_6|^2-|f_7|^2)$$
$$+4M_\phi^2(|f_1|^2-|f_4|^2))+2\lambda(q^2-2m_l^2)(|f_2|^2+f_2f_3^*(q^2-M_{B_s}^2+M_\phi^2))+2\lambda^2|f_6|^2(q^2-10m_l^2)\}, \quad (63)$$

$$P_{\rm NN} \propto -\frac{1}{3M_\phi^2q^2}\{48|f_2|^2m_l^2M_\phi^2q^2-4m_l^2(M_{B_s}^2-M_\phi^2)(|f_5|^2+(f_3f_2^*-f_6f_5^*))+(4m_l^2+M_B^2)f_6f_5^*+12m_l^2f_5f_7^*$$
$$-|f_5|^2+12m_l^2M_{B_s}^2(|f_6|^2-f_6f_7^*)+4m_l^2M_\phi^2(4|f_1|^2-4|f_4|^2+3(f_6f_7^*+|f_6|^2))+f_3f_2^*(2m_l^2-M_{B_s}^2+M_\phi^2)$$
$$+6m_l^2q^2(f_7f_5^*-2f_7f_6^*(M_{B_s}^2-M_\phi^2))+q^2(f_3f_2^*-f_6f_5^*-6m_l^2(|f_7|^2+|f_6|^2)+4(|f_4|^2$$
$$-|f_1|^2))+\lambda(q^2+2m_l^2)(|f_2|^2+f_2f_3^*(q^2-M_{B_s}^2+M_\phi^2)+2\lambda^2|f_6|^2)\}, \quad (64)$$

with

$$\mathcal{U}_1 = m_l^2q^2(6M_{B_s}^2(M_\phi^2+q^2)-3(M_\phi^2-q^2)^2-3M_{B_s}^4-5\lambda)+q^2\mathcal{U}_\in, \qquad \mathcal{U}_2 = \lambda q^2-\sqrt{q^2(q^2-4m_l^2)}u\sqrt{\lambda},$$
$$\mathcal{U}_3 = 6(M_{B_s}^6-M_\phi^6)+9M_\phi^4q^2-3q^6-3M_{B_s}^4(6M_\phi^2+5q^2)$$
$$+M_{B_s}^2(18M_\phi^4+6q^2M_\phi^2+12q^4-\lambda)+\lambda(M_{B_s}^2+M_\phi^2)+q^2(M_{B_s}^2-M_\phi^2-q^2)\mathcal{U}_2,$$
$$\mathcal{U}_4 = 6(M_{B_s}^2-M_\phi^2)^2-6q^2(M_{B_s}^2+M_\phi^2)+3q^4-\lambda,$$

and u and λ are defined in Eqs. (40) and (41), respectively.

We should add a few words about the lepton polarization asymmetry. We have seen that the expressions for various double-lepton polarization asymmetries are functions of q^2 and the parameters of NP models. From an experimental point of view, it would be more interesting if we could eliminate the dependency on one parameter, and this we can easily do by performing an integration on q^2. This will give us the average lepton polarization asymmetry, which is defined as

$$\langle P_{ij}\rangle = \frac{\int_{\text{all } q^2} P_{ij}\frac{dB}{dq^2}dq^2}{\int_{\text{all } q^2}\frac{dB}{dq^2}dq^2}. \quad (65)$$

E. Helicity fractions of ϕ in $B_s \to \phi\ell^+\ell^-$

We now discuss helicity fractions of ϕ in $B_s \to \phi\ell^+\ell^-$, which are interesting variables and are as such independent of the uncertainties arising due to form factors and other input parameters. The final-state meson helicity fractions were already discussed in the literature for $B \to K^*(K_1)\ell^+\ell^-$ decays [88,89].

The explicit expression of the decay rate for $B_s^- \to \phi\ell^+\ell^-$ decay can be written in terms of the longitudinal ($\Gamma_{\rm L}$) and transverse (Γ_T) components as

$$\frac{d\Gamma(q^2)}{dq^2} = \frac{d\Gamma_{\rm L}(q^2)}{dq^2}+\frac{d\Gamma_{\rm T}(q^2)}{dq^2}, \quad (66)$$

where

$$\frac{d\Gamma_{\rm T}(q^2)}{dq^2} = \frac{d\Gamma_+(q^2)}{dq^2}+\frac{d\Gamma_-(q^2)}{dq^2}$$

and

$$\frac{d\Gamma_{\rm L}(q^2)}{dq^2} = \frac{G_F^2|V_{tb}V_{ts}^*|^2\alpha^2}{2^{11}\pi^5}\frac{u(q^2)}{M_{B_s}^3}\times\frac{1}{3}\mathcal{A}_{\rm L}, \quad (67)$$

$$\frac{d\Gamma_{\pm}(q^2)}{dq^2} = \frac{G_F^2|V_{tb}V_{ts}^*|^2\alpha^2}{2^{11}\pi^5}\frac{u(q^2)}{M_{B_s}^3}\times\frac{4}{3}\mathcal{A}_{\pm}. \quad (68)$$

The different functions appearing in Eqs. (67) and (68) can be expressed in terms of auxiliary functions [cf. Eqs. (28)–(34)] as

$$\begin{aligned}\mathcal{A}_{\rm L} = {} & \frac{1}{q^2M_\phi^2}[24|f_7(q^2)|^2m^2M_\phi^2\lambda \\ & + (2m^2+q^2)|(M_{B_s}^2 - M_\phi^2 - q^2)f_2(q^2) \\ & + \lambda f_3(q^2)|^2 + (q^2-4m^2)|(M_{B_s}^2 - M_\phi^2 - q^2)f_5(q^2) \\ & + \lambda f_6(q^2)|^2], \end{aligned} \quad (69)$$

$$\begin{aligned}A_{\pm} = {} & (q^2-4m^2)|f_5(q^2) \mp \sqrt{\lambda}f_4(q^2)|^2 \\ & + (q^2+2m^2)|f_2(q^2) \pm \sqrt{\lambda}f_1(q^2)|^2. \end{aligned} \quad (70)$$

Finally, the longitudinal and transverse helicity amplitudes become

$$f_{\rm L}(q^2) = \frac{d\Gamma_{\rm L}(q^2)/dq^2}{d\Gamma(q^2)/dq^2}, \qquad f_{\pm}(q^2) = \frac{d\Gamma_{\pm}(q^2)/dq^2}{d\Gamma(q^2)/dq^2},$$
$$f_{\rm T}(q^2) = f_+(q^2) + f_-(q^2), \quad (71)$$

so that the sum of the longitudinal and transverse helicity amplitudes is equal to one, i.e., $f_{\rm L}(q^2) + f_{\rm T}(q^2) = 1$ for each value of q^2 [23].

V. NUMERICAL ANALYSIS

In this section we will examine the above derived physical observables and analyze the effects of different new physics scenarios on them. The form factors are nonperturbative quantities and for them we rely on the LCSR approach for the numerical calculations. The numerical values of the LCSR form factors along with the different fitting parameters [52] are summarized in Table I. In addition to the parameters corresponding to different NP models there are some standard inputs, which are collected in Table III.

The strength of the other NP parameters that correspond to the UED and Z' models are varied such that they lie inside the bounds given by different flavor decays observed so far. We emphasize here that in all the figures the band corresponds to the uncertainties in different input parameters where form factors are the main contributors (c.f. Table I) and we have defined $q^2 = s$. The NP curves are plotted by varying the values of NP parameters in the range summarized in Table IV.

TABLE III. Default values of input parameters used in the calculations.

$m_{B_s} = 5.366$ GeV, $m_b = 4.28$ GeV, $m_s = 0.13$ GeV, $m_\mu = 0.105$ GeV, $m_\tau = 1.77$ GeV, $f_B = 0.25$ GeV, $\lvert V_{tb}V_{ts}^*\rvert = 45\times10^{-3}$, $\alpha^{-1} = 137$, $G_F = 1.17\times10^{-5}$ GeV^{-2}, $\tau_B = 1.54\times10^{-12}$ sec, $m_\phi = 1.020$ GeV.

TABLE IV. The numerical values of the Z' parameter.

	$\lvert B_{sb}\rvert\times10^{-3}$	$\phi_{sb}[^\circ]$	$S_{\rm LL}\times10^{-2}$	$D_{\rm LL}\times10^{-2}$
$\mathcal{S}_1$	1.09 ± 0.22	-72 ± 7	-2.8 ± 3.9	-6.7 ± 2.6
$\mathcal{S}_2$	2.20 ± 0.15	-82 ± 4	-1.2 ± 1.4	-2.5 ± 0.9

Semileptonic B_s decay are ideal probes to study physics in and beyond the Standard Model. In this context, there are a large number of observables which are accessible in these decays. However, in general the branching ratio for semileptonic decays is prone to many sources of uncertainties. The major source of uncertainty originates from the $B\to\phi$ transition form factors that can cause a roughly 20–30% uncertainty in the differential branching ratio. This goes to show that the differential branching ratio may not be a suitable observable to look for NP effects unless these effects are very drastic. In the absence of the precise form factors, it is still possible to constraint new physics with the help of observables that exhibit reduced sensitivity to the form factors. In this regard the most important observables are the zero position of the forward-backward asymmetry, different lepton polarization asymmetries, and the helicity fractions of the final-state meson. This will become clear in Figs. 2–14, where we will see that the gray band corresponding to the uncertainties in different input parameters totally shrinks.

The SM predicts the zero crossing of $\mathcal{A}_{\rm FB}(q^2)$ at a well-determined position that is free from the hadronic uncertainties at the LO in the strong coupling α_s [12–14]. For this reason, the zero position of $A_{\rm FB}$ is an important observable in the search for new physics. In order to make this point clear, the zero position (q_0^2) is just the root of Eq. (46), which can be written as

$$\begin{aligned}q_0^2 = {} & -\frac{C_7^{\rm eff}}{\Re(C_9^{\rm eff}(q_0^2))}m_b \\ & \times\left[\frac{T_2(q_0^2)}{A_1(q_0^2)}(M_{B_s}-M_\phi) + \frac{T_1(q_0^2)}{V(q_0^2)}(M_{B_s}+M_\phi)\right]. \end{aligned} \quad (72)$$

It is really spectacular that for the $B\to Vl^+l^-$ decays, we can find that with the use of effective theories like soft-collinear effective theory both ratios of the form factors appearing in Eq. (72) have no hadronic uncertainty, i.e., all dependence on the intrinsically nonperturbative quantities cancels. Therefore, one can simply write

$$\frac{T_2(q^2)}{A_1(q^2)} = \frac{M_{B_s}}{M_{B_s}-M_\phi}, \qquad \frac{T_1(q^2)}{V(q^2)} = \frac{M_{B_s}}{M_{B_s}+M_\phi},$$

and by using these relations the short-distance expression for the zero position of $\mathcal{A}_{\rm FB}$ is given by [13]

TABLE V. Branching ratio of $B_s \to \phi l^+ l^-$ in the SM and different NP scenarios. The central values of the form factors and other input parameters are used.

Model	$B_s \to \phi \mu^+ \mu^-$	$B_s \to \phi \tau^+ \tau^-$
SM	1.58×10^{-6}	2.37×10^{-7}
UED	0.91×10^{-6}	0.94×10^{-6}
$Z'-$	1.86×10^{-6}	3.07×10^{-7}

$$q_0^2 = \frac{2 m_b M_{B_s}}{\Re[C_9^{\rm eff}(q_0^2)]} C_7^{\rm eff}. \tag{73}$$

Recently LHCb published its results on $\mathcal{A}_{\rm FB}(\bar{B} \to \bar{K}^* \mu^+ \mu^-)$ which show, with small error bars, that the zero position of $\mathcal{A}_{\rm FB}(\bar{B} \to \bar{K}^* \mu^+ \mu^-)$ is close to the SM's zero position. Like $\bar{B} \to \bar{K}^* \mu^+ \mu^-$ decay, the semileptonic decay $B_s \to \phi \mu^+ \mu^-$ also occurs through the quark-level transition $b \to s \mu^+ \mu^-$. Therefore, future measurements of the $\mathcal{A}_{\rm FB}(B_s \to \phi \mu^+ \mu^-)$ will shed more light on NP in the flavor sector.

The other ''optimized'' observables are the various polarization asymmetries attached to the final-state leptons and meson, where the uncertainties are also mild. In this regard the longitudinal and normal lepton polarization asymmetries are a good tool to probe the NP. On the other hand, the transverse lepton polarization asymmetry [c.f. Eq. (53)] is proportional to the imaginary part of the auxiliary functions and hence will be negligible in the models where we have real couplings. In addition to the single-lepton polarization, we will also discuss the dependence of double-lepton polarization asymmetries on q^2 and will also give the numerical values of their averages, which can be obtained after an integration on q^2.

Another interesting observable in this list is the study of the spin effects of the final-state meson, which for our case is the ϕ meson. A detailed discussion about the NP effects on the longitudinal and transverse helicity fractions has been done in the forthcoming numerical analysis, which will allow us to uncover the potential of various NP scenarios.

Similarly, the polarized and unpolarized CP-violating asymmetries are a useful tool in finding the distinguishing features from the SM as well as helping us to segregate the two NP models. It is worth mentioning that the FCNC transitions are proportional to the CKM matrix elements, $V_{tb} V_{ts}^*$, $V_{cb} V_{cs}^*$, and $V_{ub} V_{us}^*$, where the latter two are highly suppressed compared to $V_{tb} V_{ts}^*$. This will eventually suppress the value of CP-violation asymmetries in the SM and also in the UED model. Because of the extra phase in the Z' model we are expecting a prominent deviation. Therefore, the study of the CP-violation asymmetries will provide key evidence of the NP coming through the extra Z' boson. This will be discussed in a separate paper [90].

The only free parameter in the UED model is the inverse of the compactification radius, i.e., $1/R$. Taking into account the LO contributions due to the exchange of KK modes as well as already available next-to-next-to-leading order corrections to $B \to X_s \gamma$, Haisch *et al.* [91] have determined that the lower bound on the inverse of the compactification radius is 600 GeV. Using the electroweak precision measurements and also some cosmological constraints, the lower limit on the inverse of the compactification radius is found to be in or above the 500 GeV range [92,93]. It is well known that by increasing $1/R$ the values of different physical observables come closer to their SM values. Therefore, in our numerical analysis we take the value of $1/R$ to be 500 GeV just to see the maximum possible deviation from the SM value.

On the other hand, the effects of the family nonuniversal Z' boson on the $b \to s$ transition have attracted much more attention and have been widely studied, where it is argued that the behavior of a family nonuniversal Z' boson is helpful to resolve many puzzles in B-meson decays, such as the πK puzzle and anomalous $\bar{B}_s - B_s$ mixing [94–98]. In the literature the differential decay width and forward-backward asymmetry of $B_s \to \phi \mu^+ \mu^-$ decay have been studied in the Z' model using three different scenarios which correspond to different values of the left- and right-handed couplings of Z' with leptons, i.e., $S_{\rm LL}$ and $D_{\rm LL}$, as well as the right-handed coupling with quarks, i.e., B_{sb} and these are collected in Table IV [98]. In the present study we will use these limits to study their impact on the branching ratio and on the various asymmetries mentioned above.

The numerical results of the branching ratios, the forward-backward asymmetry, the different polarization asymmetries of the final-state leptons, and the helicity fractions of the final-state ϕ meson as a function of q^2 in $B_s \to \phi l^+ l^-$ decays are presented in Figs. 1–14. Figures 1(a) and 1(b) describe the differential branching ratio of $B_s \to \phi \mu^+ \mu^- (\tau^+ \tau^-)$ decay, where one can see that—for the choice of the parameters made in accordance with the current data on various flavor physics decay modes—our results lie close to the SM predictions. This can also be summarized in Table V. We should mention that when we have muons as the final-state leptons [cf. Fig. 1(a)] the bands for two Z' scenarios overlap. We can also see that the value of the branching ratio lies well within the range of the experimental limits for different choices for the values of NP parameters, and one can notice that the NP contributions are overshadowed by the uncertainties involved in different input parameters. Therefore, to look for NP we have to calculate the observables where hadronic uncertainties almost have no effect and which are almost independent of the choice of form factors. Among them the most pertinent are the zero position of the forward-backward asymmetry, the lepton polarization asymmetries, the helicity fractions of the final-state meson, and CP asymmetries, which are almost free from the hadronic uncertainties and serve as handy tools for extracting an NP signature. This is clear from Figs. 2–14,

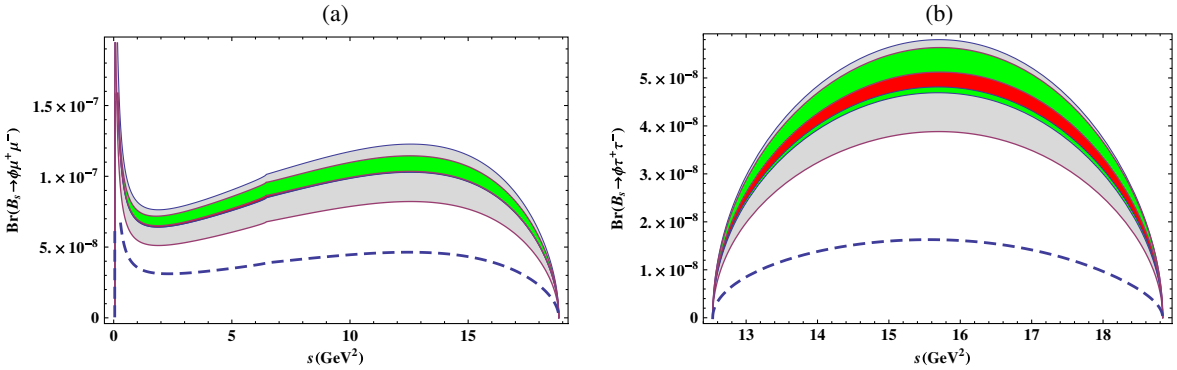

FIG. 1 (color online). The differential width for the $B_s \to \phi l^+ l^-$ ($l = \mu, \tau$) decays as functions of $q^2 = s$. The gray, green, and red bands correspond to the Standard Model, and Z' scenarios S_1 and S_2, respectively. The dashed blue line corresponds to the UED model.

where the gray band, corresponding to the uncertainties in the form factors and other input parameters of the SM, is too narrow.

As we have already mentioned, at the leading order in the strong coupling constant α_s in the SM the destructive interference between the photon penguin (C_7^{eff}) and the Z penguin (C_9^{eff}) make the forward-backward asymmetry equal to zero at a particular position which is independent of the form factors, as depicted in Eq. (73). For the decay $B_s \to \phi \mu^+ \mu^-$, the value of the zero crossing is approximately $q^2 \simeq 1.6\ \mathrm{GeV}^2$. The deviation of the zero crossing from the SM value gives us some clues for the NP. Figure 2(b) shows the effect of various NP scenarios on the zero position of the forward-backward asymmetry for $B_s \to \phi \mu^+ \mu^-$ decay. Working with $B \to K^* l^+ l^-$, where the experimental results of LHCb lie close to the SM

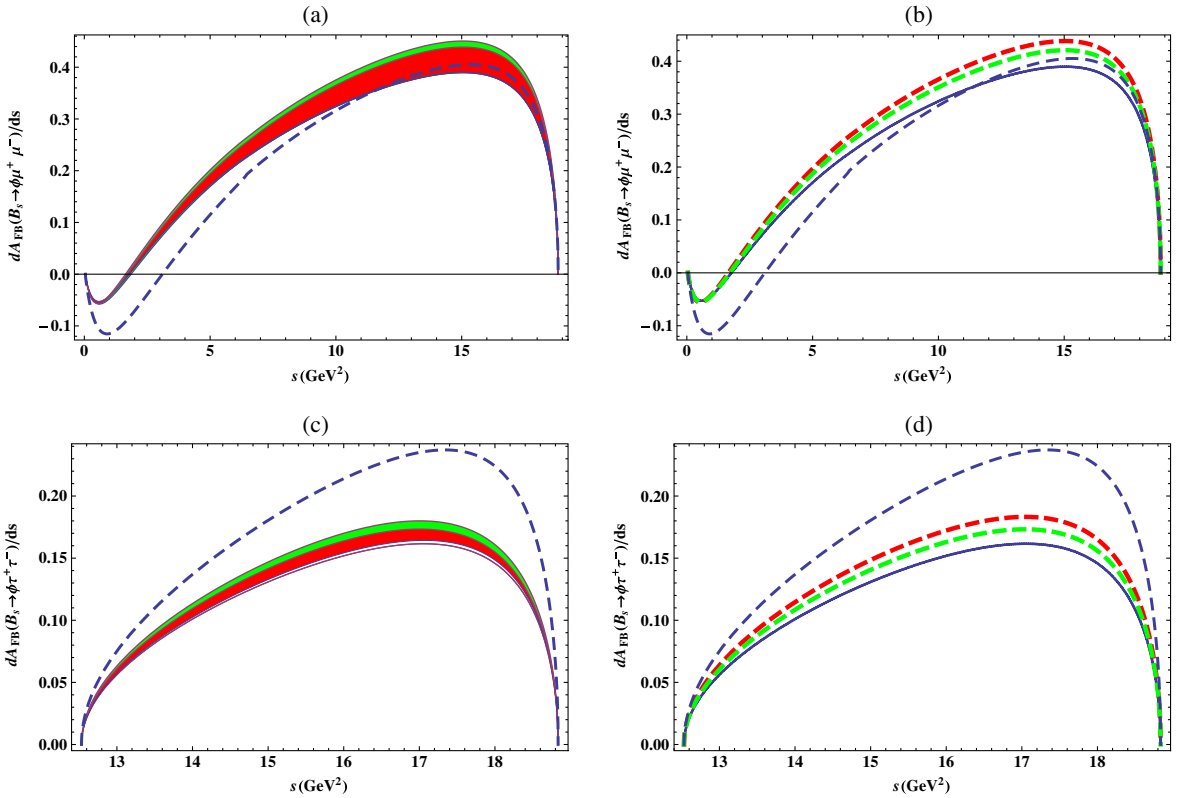

FIG. 2 (color online). The differential forward-backward asymmetry for the $B_s \to \phi l^+ l^-$ ($l = \mu, \tau$) decays as functions of q^2. The gray, green (light gray), and red (dark gray) bands correspond to the Standard Model, and Z' scenarios S_1 and S_2, respectively. The dashed blue line corresponds to the UED model. In (b) and (d) the solid, thin dashed blue, thick dashed green (light gray), and thick dashed red (dark gray) lines correspond to the SM, the UED model, and the Z'-model scenarios I and II, respectively. The figures in the right panel are plotted for central values of the form factors and other input parameters.

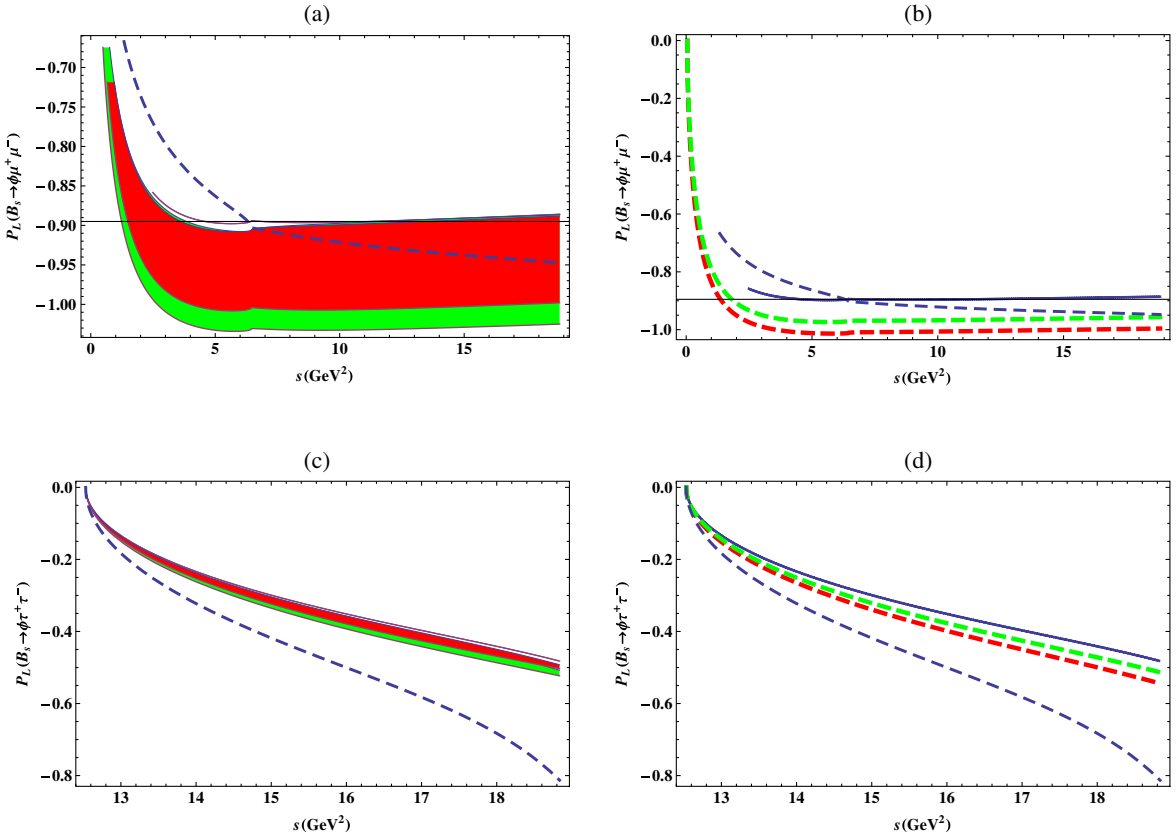

FIG. 3 (color online). The longitudinal lepton polarization asymmetry for the $B_s \to \phi l^+ l^-$ ($l = \mu, \tau$) decays as functions of q^2. The legends are the same as in Fig. 2.

value, we can see that only a small deviation from the SM zero position of $\mathcal{A}_{\text{FB}}$ arises in case of the Z' model. In the case of the UED model the value of the Wilson coefficient C_7 is significantly reduced, whereas C_9 almost remains unaltered for $1/R = 500$ GeV. By looking at Eq. (73) we can see that the zero position is directly proportional to C_7, and therefore we expect a large deviation in the UED model, which is obvious from Fig. 2(b). We expect that future data from the LHCb measurement of the forward-backward asymmetry in $B_s \to \phi\mu^+\mu^-$ will help us in observing new physics and will also give us an opportunity to distinguish between various NP scenarios.

It has been pointed out by Beneke *et al.* [14] that the next-to-leading order corrections to the lepton invariant mass spectrum in $B \to K^* l^+ l^-$ is small, but there is a large correction to the predicted location of the zero position of the forward-backward asymmetry which is estimated to be 30%. Such a calculation must be performed for the $B_s \to \phi l^+ l^-$ decays before one can say anything about the NP by measuring forward-backward asymmetry in these decays.

Figures 3(a)–3(d) show the dependence of the longitudinal lepton polarization asymmetry for the $B_s \to \phi l^+ l^-$ decay on the square of the momentum transfer for different NP models. In case of the UED model, the value of the longitudinal lepton polarization lies close to the SM value, where a significant deviation is obtained in the case of the Z' model. This can also be seen quantitatively from Table VI, where an 11% deviation is observed in the case of the Z' model for the central values of its parameters.

Figures 4(a)–4(d) display the behavior of the normal lepton polarization asymmetry for $B_s \to \phi l^+ l^-$ with the square of the momentum transfer in the SM and in NP models. From Eq. (52) one can see that it is proportional to the mass of the leptons. Therefore, when we have muons as final-state leptons we can see that its SM value and the deviation from this value through NP are only significant in the low-q^2 region and that these effects are almost vanish when we increase the value of q^2. Similarly, we have drawn the normal lepton polarization asymmetry when τ's are the final-state leptons in Figs. 6(c) and 6(d). We can see that in the SM the value of the normal lepton polarization asymmetry is positive throughout almost the entire kinematical region. It can be easily seen that the value in the Z' model is also quite different from that of the SM value. The most interesting effect comes in the UED model where the value of this asymmetry is negative in almost the entire available q^2 range. Hence it will be a

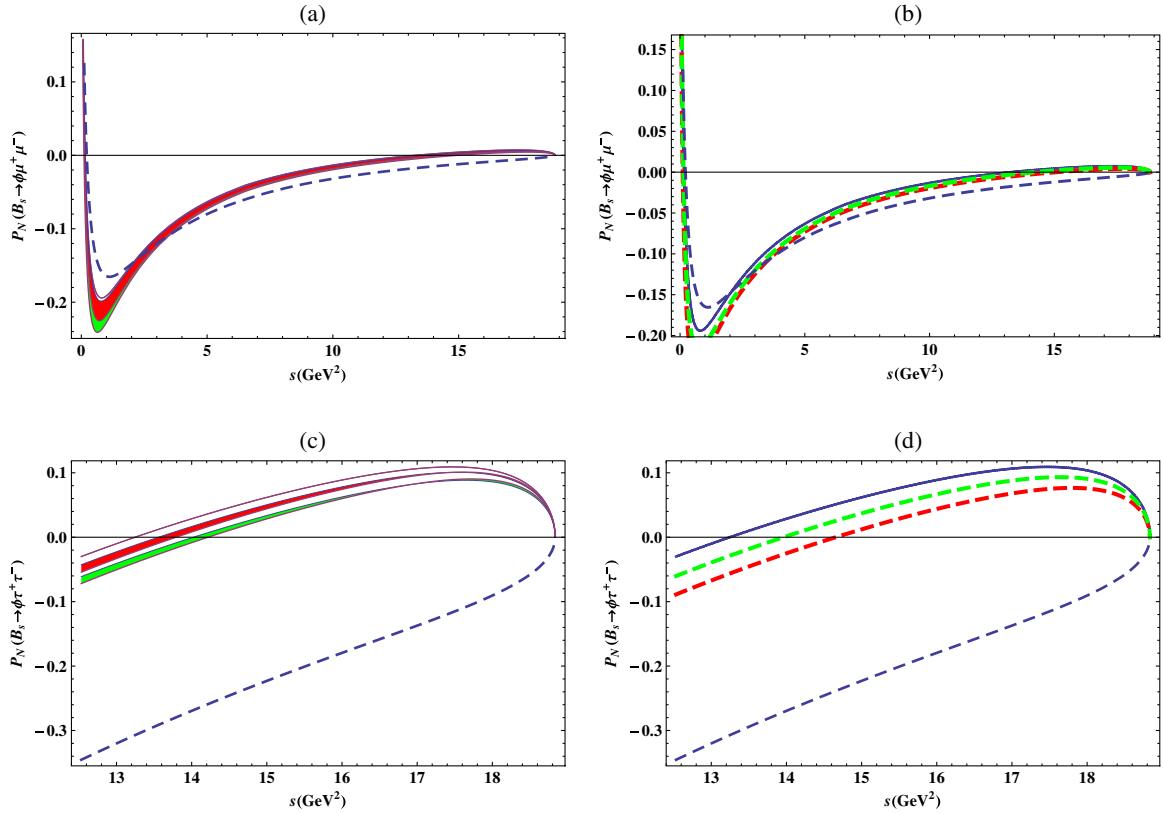

FIG. 4 (color online). The normal lepton polarization asymmetry $B_s \to \phi l^+ l^-$ ($l = \mu, \tau$) decays as functions of q^2. The legends are the same as in Fig. 2.

clear signal of new physics and by measuring its sign we can distinguish between the NP models under consideration.

Just like the normal lepton polarization asymmetry the transverse lepton polarization asymmetry is also proportional to the lepton mass. In addition to this it is also proportional to the imaginary part of the combination of different auxiliary functions and therefore the Wilson coefficients as well. The Wilson coefficients remain real in the SM and the UED model but not in the Z' model. However, in this model the imaginary part is also too small. Hence the value of the transverse lepton polarization asymmetry remains too small to be measured, and Figs. 5(a) and 5(b) portray this fact.

The dependence of various double-lepton polarization asymmetries on q^2 for the aforementioned decay in the SM and various NP scenarios is given in Figs. 6–12. In Figs. 6(a)–6(d) we have plotted P_{LL} as a function of q^2. It is

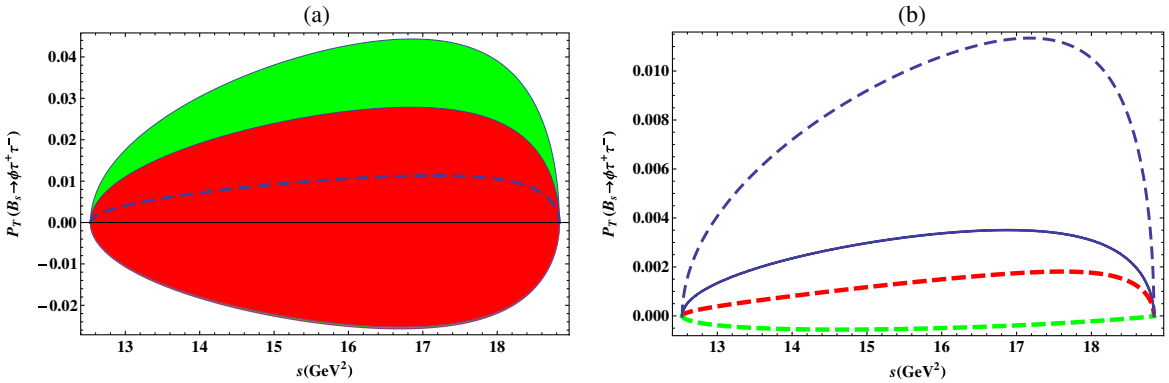

FIG. 5 (color online). The transverse lepton polarization asymmetry for $B_s \to \phi\tau^+\tau^-$ decays as a functions of q^2. The legends are the same as in Fig. 2.

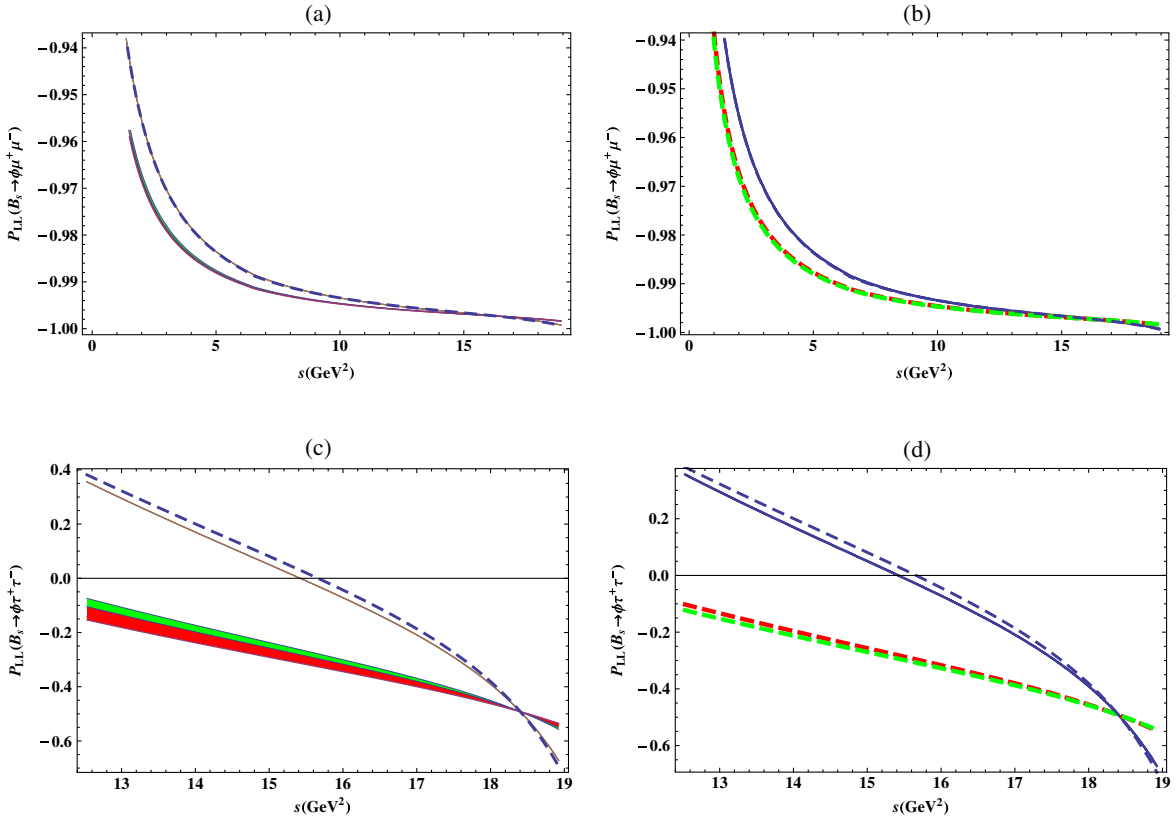

FIG. 6 (color online). P_{LL} for the $B_s \to \phi l^+ l^-$ ($l = \mu, \tau$) decays as functions of q^2. The legends are the same as in Fig. 2.

clear from Eq. (58) that the double longitudinal lepton polarization asymmetry is proportional to the inverse of the mass of the lepton, and therefore it is expected to have a large value when the final-state leptons are muons compared to the case when we have τ's, and it is also clear from the figures. We can also see that the dependency of P_{LL} on NP parameters is small for the μ channel. However, for the τ channel the maximum shift comes in the Z' model where $\langle P_{\text{LL}} \rangle$ deviates by almost an order of magnitude from the SM value (cf. Table VII). Its measurement will help us in identifying the NP effects arising due to the extra gauge boson in the Z' model.

By looking at Eq. (7), we can see that P_{LN} is proportional to the imaginary part of the different auxiliary functions and therefore the Wilson coefficients as well; therefore, its nonzero value is expected only in the Z' model. However, the imaginary part in this case is small, and therefore its values is expected to be small. Figures 7(a) and 7(b) display this fact, which quantitatively can also be seen in Table VII.

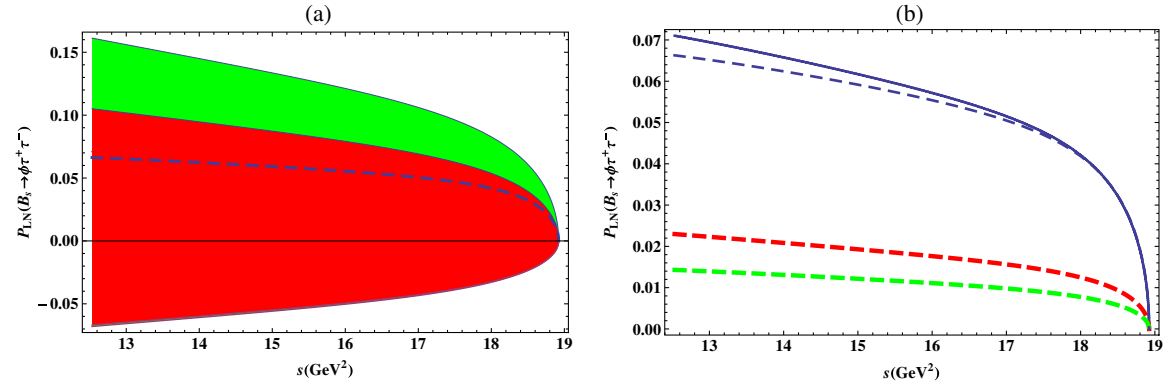

FIG. 7 (color online). P_{LN} for the $B_s \to \phi l^+ l^-$ ($l = \mu, \tau$) decays as functions of q^2. The legends are the same as in Fig. 2.

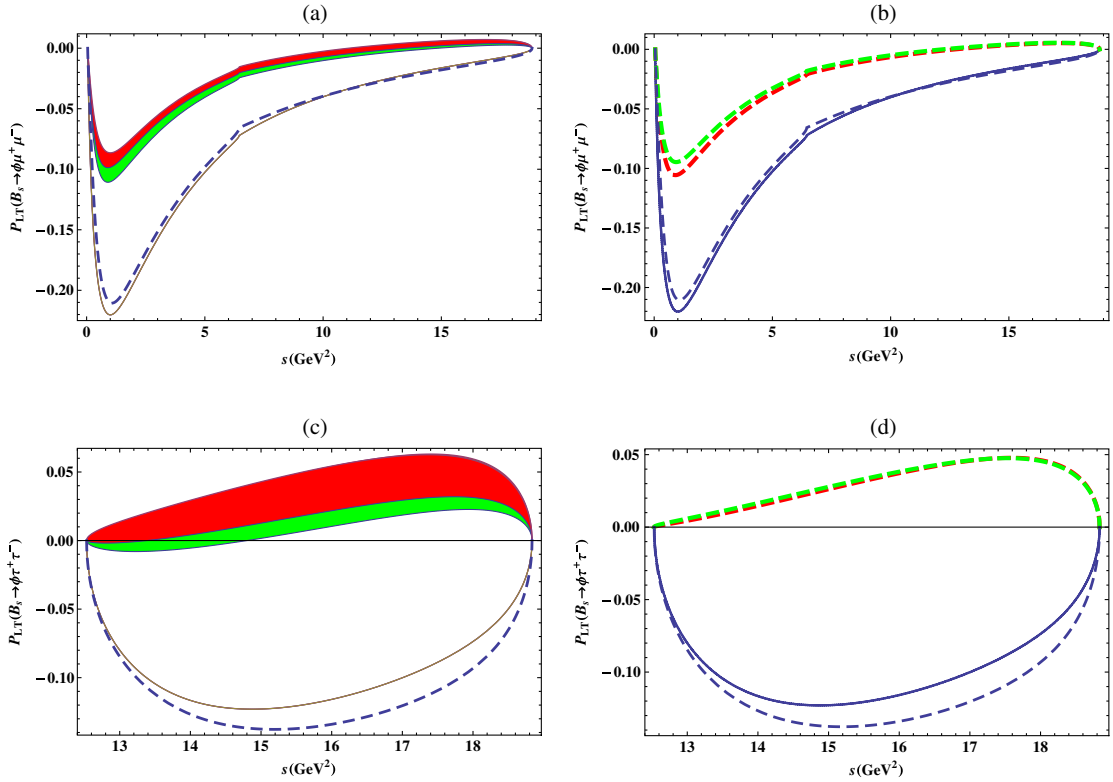

FIG. 8 (color online). P_{LT} for the $B_s \to \phi l^+ l^-$ $(l = \mu, \tau)$ decays as functions of q^2. The legends are the same as in Fig. 2.

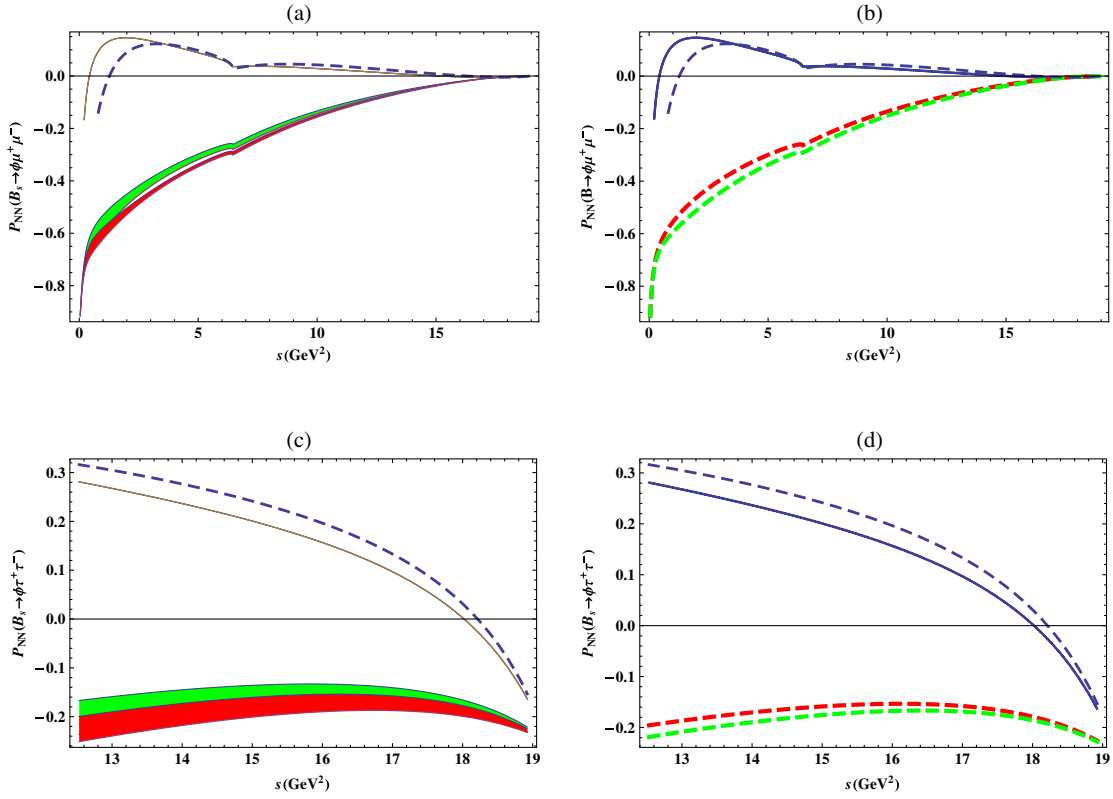

FIG. 9 (color online). P_{NN} for the $B_s \to \phi l^+ l^-$ $(l = \mu, \tau)$ decays as functions of q^2. The legends are the same as in Fig. 2.

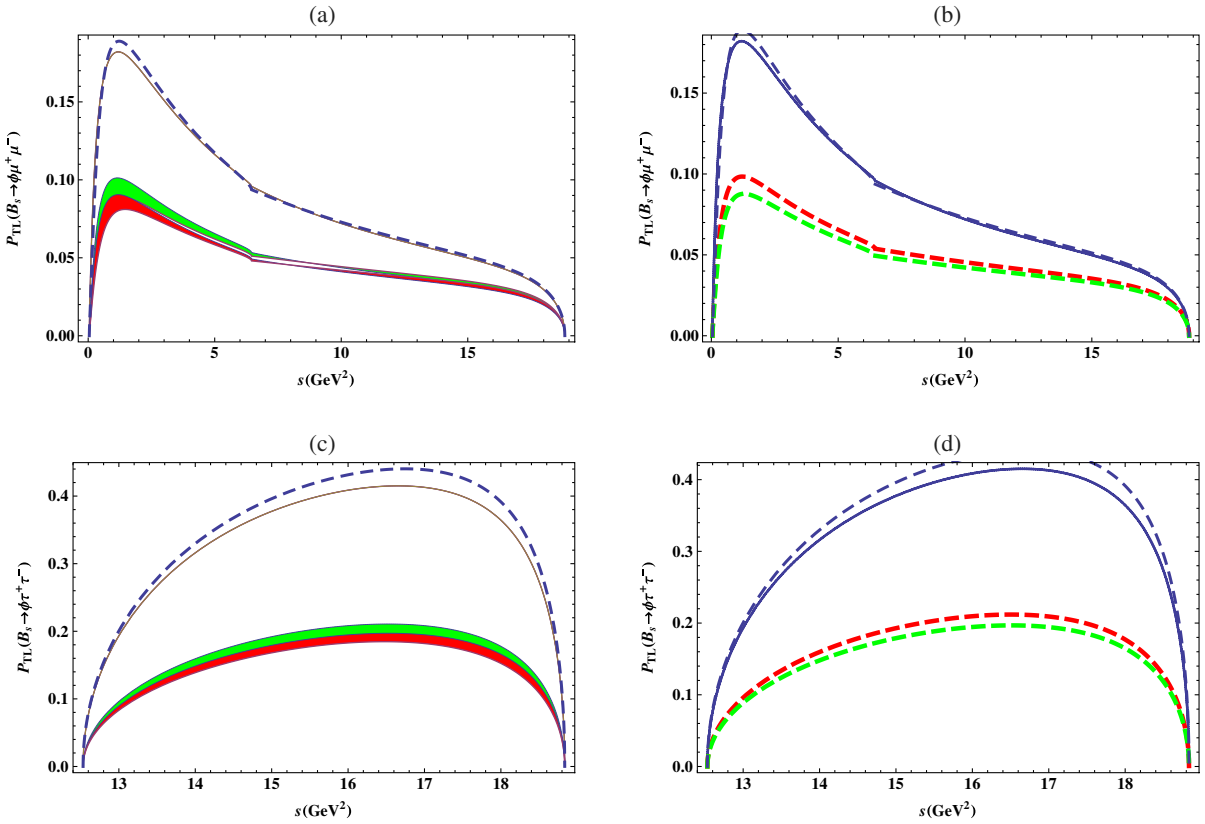

FIG. 10 (color online). P_{TL} for the $B_s \to \phi l^+ l^-$ ($l = \mu, \tau$) decays as functions of q^2. The legends are the same as in Fig. 2.

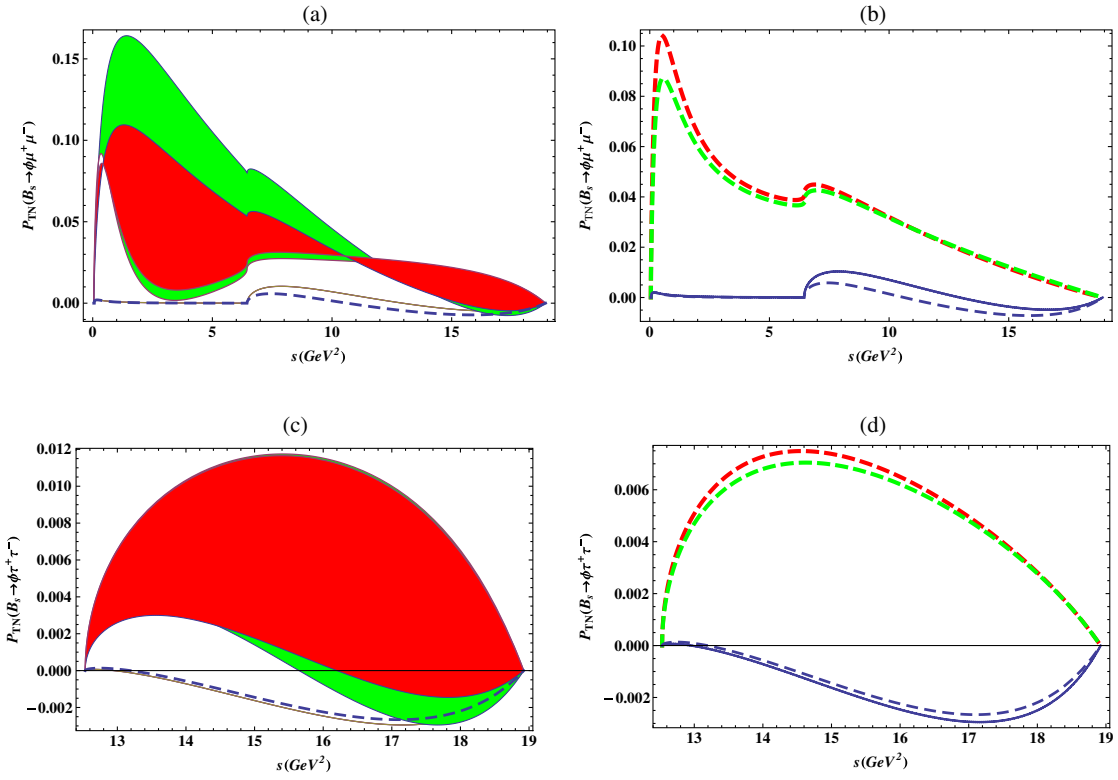

FIG. 11 (color online). P_{TN} for the $B_s \to \phi l^+ l^-$ ($l = \mu, \tau$) decays as functions of q^2. The legends are the same as in Fig. 2.

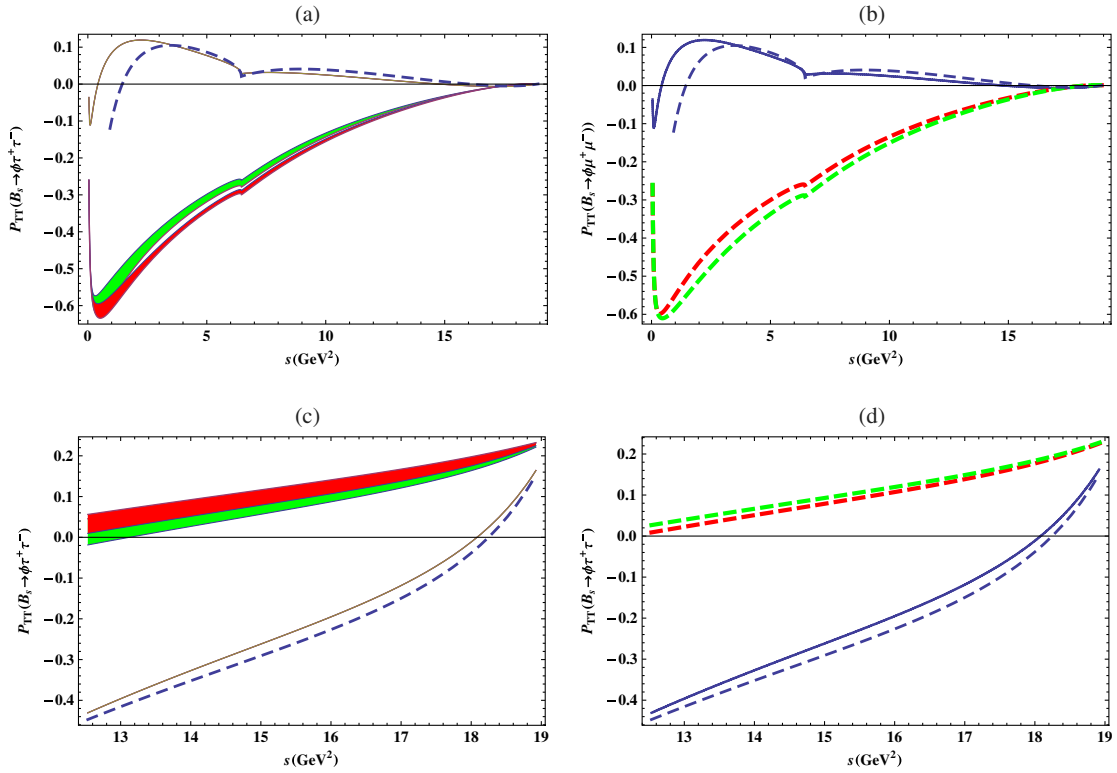

FIG. 12 (color online). P_{TT} for the $B_s \to \phi l^+ l^-$ ($l = \mu, \tau$) decays as functions of q^2. The legends are the same as in Fig. 2.

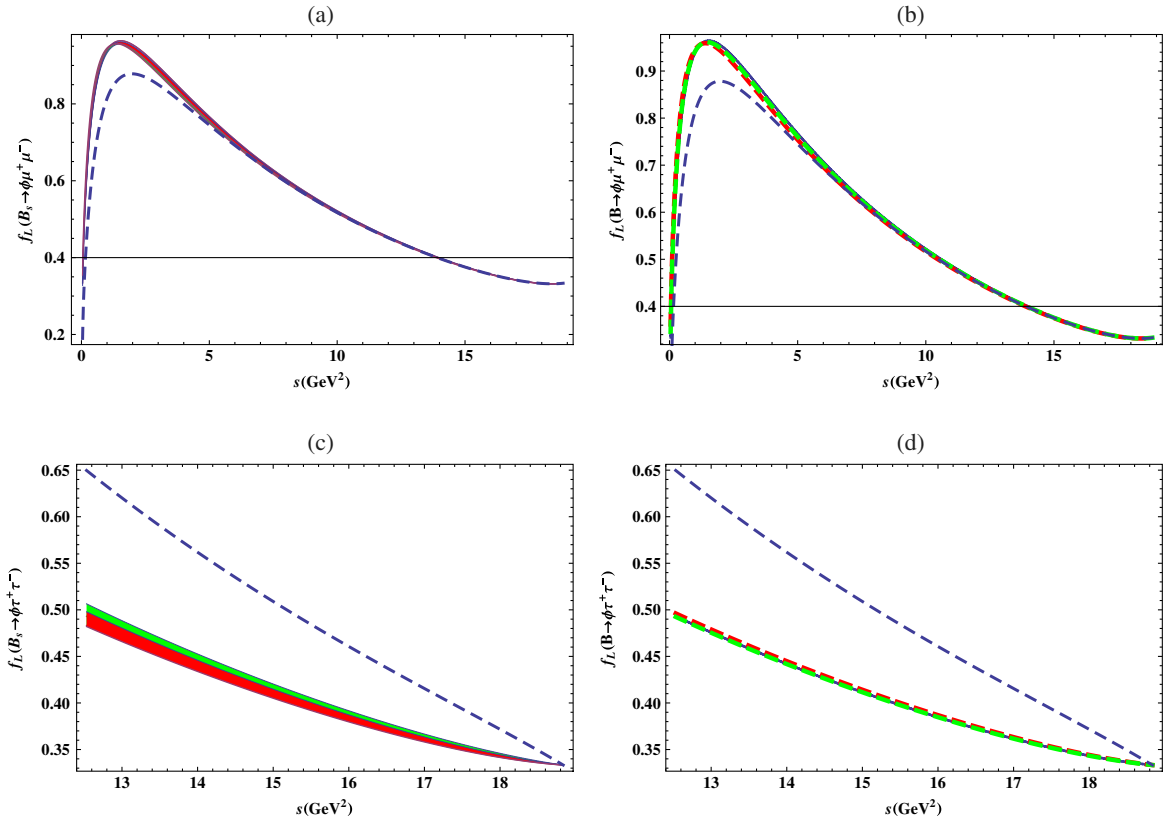

FIG. 13 (color online). The longitudinal helicity fractions for the $B_s \to \phi l^+ l^-$ ($l = \mu, \tau$) decays as functions of q^2. The legends are the same as in Fig. 2.

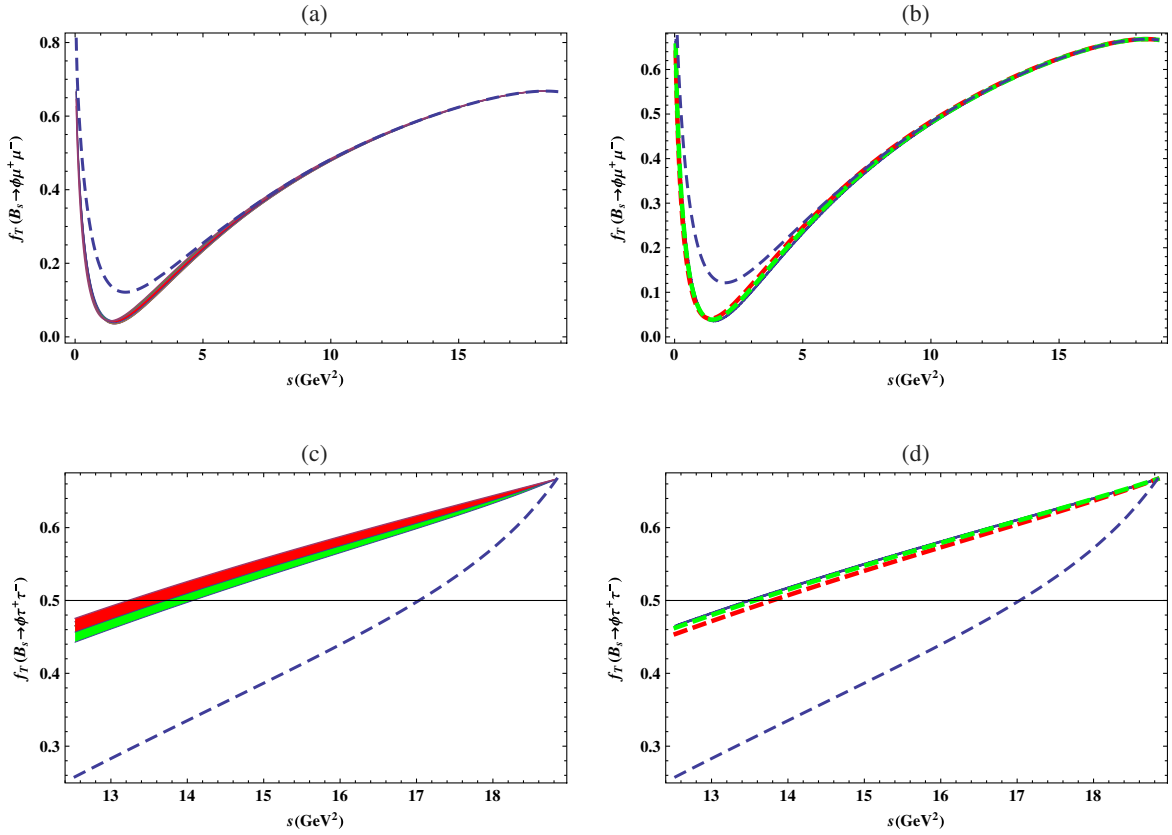

FIG. 14 (color online). The transverse helicity fractions for the $B_s \to \phi l^+ l^-$ ($l = \mu, \tau$) decays as functions of q^2. The legends are the same as in Fig. 2.

Figures 8(a)–8(d) depict the behavior of P_{LT} with q^2, where we can see that the new physics effects are quite promising both for the μ and τ channels in almost the whole range of available q^2. Quantitatively we can see from Table VII that the average value $\langle P_{\mathrm{LT}} \rangle$ in the UED model is close to the SM value, whereas in the Z' model the average value of P_{LT} is significantly suppressed in magnitude from its SM value in addition to having its sign flipped for the τ channel.

In Figs. 9(a)–9(d) we display the effects of various NP models on P_{NN}. We can see that the value of P_{NN} shows a strong dependence on the parameters of NP, which is quite prominent in both the μ and τ channels. From Table VII, it is clear that in the Z' model the value of P_{NN} is significantly different not only from the SM value but also from the UED model. Therefore the experimental observation of this observable will help us to segregate the Z' model from both the SM as well as from the UED model.

The situation for P_{TL} is not so interesting for the μ channel because its average value is small in this case. However, when we have τ's as final-state leptons, the effects of the extra gauge boson in the Z' model reduce the average value of P_{TL} by 50%. This can be seen quantitatively from Table VII and it is also depicted in Figs. 10(a)–10(d).

In Eq. (11) we can see that the value of P_{TN} comes from the imaginary part of various Wilson Coefficients, and therefore—as expected—its value is too small to measure. This is obvious from Figs. 10(a)–10(d) and also from Table VII.

TABLE VI. Average values of various single-lepton polarizations for the central values of the form factors. The values in the bracket are for the $\tau^+\tau^-$ channel. The upper (lower) values correspond to the upper (lower) limits of the two Z' scenarios.

Model	$\langle P_{\mathrm{L}} \rangle$	$\langle P_{\mathrm{N}} \rangle$	$\langle P_{\mathrm{T}} \rangle$
SM	$-0.859(-0.322)$	$-0.0334(0.068)$	$0.0003(0.0028)$
UED	$-0.857(-0.462)$	$-0.0451(-0.197)$	$0.0007(0.0091)$
$Z'(S_1)$	$-0.972^{+0.108}_{-0.024}(-0.365^{+0.031}_{+0.075})$	$-0.0445^{+0.007}_{-0.001}(0.023^{+0.019}_{+0.016})$	$-0.0005^{+0.005}_{-0.004}(0.0012^{+0.035}_{-0.023})$
$Z'(S_2)$	$-0.931^{0.066}_{-0.037}(-0.346^{+0.018}_{-0.001})$	$-0.040^{+0.001}_{-0.002}(0.046^{+0.012}_{+0.009})$	$-0.0006^{+0.004}_{-0.0036}(-0.0004^{+0.0023}_{-0.021})$

TABLE VII. Average values of various double-lepton polarizations for the central values of the form factors. The values in the bracket are for the $\tau^+\tau^-$ channel. The upper (lower) values correspond to the upper (lower) limits of the two Z' scenarios.

	SM	UED	Z' (S_1 scenario)	Z' (S_2 scenario)
$\langle P_{LL}\rangle$	$-0.956(-0.046)$	$-0.939(-0.017)$	$-0.961^{+0.003}_{-0.001}(-0.30^{+0.02}_{-0.025})$	$-0.959^{+0.001}_{-0.006}(-0.313^{+0.011}_{-0.058})$
$\langle P_{NN}\rangle$	0.014(0.153)	$-0.066(0.192)$	$-0.241^{+0.002}_{-0.014}(-0.166^{+0.021}_{-0.029})$	$-0.265^{+0.005}_{-0.005}(-0.181^{+0.014}_{-0.023})$
$\langle P_{TT}\rangle$	$0.025(-0.207)$	$-0.037(-0.237)$	$-0.218^{+0.005}_{-0.013}(0.102^{-0.021}_{+0.026})$	$-0.238^{+0.005}_{-0.042}(0.114^{-0.013}_{+0.046})$
$\langle P_{LN}\rangle$	0.0027(0.057)	0.0023(0.055)	$0.0028^{+0.021}_{-0.0138}(0.017^{+0.104}_{-0.067})$	$0.0014^{+0.014}_{-0.002}(0.011^{+0.068}_{-0.060})$
$\langle P_{LT}\rangle$	$-0.069(-0.104)$	$-0.070(-0.104)$	$-0.022^{-0.004}_{+0.003}(0.030^{-0.037}_{+0.015})$	$-0.019^{-0.003}_{+0.002}(0.031^{-0.014}_{+0.014})$
$\langle P_{TL}\rangle$	0.085(0.356)	0.084(0.356)	$0.050^{-0.001}_{-0.003}(0.180^{-0.001}_{-0.016})$	$0.045^{+0.0001}_{-0.0001}(0.167^{+0.0001}_{-0.011})$
$\langle P_{TN}\rangle$	$0.0016(-0.0018)$	$-0.007(-0.0015)$	$0.039^{+0.023}_{-0.011}(0.0058^{-0.0057}_{+0.004})$	$0.037^{+0.007}_{-0.006}(0.0055^{-0.0054}_{+0.004})$

The case in which both the leptons are transversely polarized—that is, P_{TT}—becomes important for the τ channel. Here we can see that its behavior with q^2 is very different in the Z' model—where it has positive values—compared to its values in the SM and in the UED model, where the value of P_{TT} is negative. This fact is depicted in Figs. 12(a)–12(d) and numerically given in Table VII.

The longitudinal (f_L) and the transverse (f_T) helicity fractions of the final-state ϕ meson are depicted in Figs. 13 and 14. In Fig. 13 one can see that the values of longitudinal helicity fractions shift significantly for some of the NP scenarios when we have τ's as the final-state particles. The maximum deviation comes in the UED model and the reason is the significant modification of the Wilson coefficients C_7 and C_9 in this model compared to their SM values. Similar effects can also be seen in case of the transverse helicity fractions.

Just to summarize, in the present study we have observed the sizeable difference between the predictions of various physical observables in the SM and two different beyond the SM scenarios, namely, the Z' and UED models. It is important to keep in mind the fact that in certain physical observables the NP effects are obscured by the uncertainties arising due to form factors, but in different lepton polarization asymmetries their effects are still considerable. We hope that the experimental study of this channel will be a valuable source for providing an indirect way to uncover the new physics effects in an indirect way.

ACKNOWLEDGMENTS

The authors would like to thank Professor Riazuddin and Professor Fayyazuddin for their valuable guidance and helpful discussions. M. J. A. would like to thank the support of Quaid-i-Azam University through the University Research Fund and M. A. P. would like to thank the support of FAPESP under the Grant No. 2012/13047-2.

[1] S. L. Glashow, J. Iliopoulos, and L. Maiani, Phys. Rev. D **2**, 1285 (1970).
[2] N. Cabibbo, Phys. Rev. Lett. **10**, 531 (1963).
[3] M. Kobayashi and K. Maskawa, Prog. Theor. Phys. **49**, 652 (1973).
[4] H. Y. Cheng, C. K. Chua, and A. Soni, Phys. Rev. D **72**, 094003 (2005).
[5] G. Buchalla, G. Hiller, Y. Nir, and G. Raz, J. High Energy Phys. 09 (2005) 074.
[6] E. Lunghi and A. Soni, J. High Energy Phys. 08 (2009) 051.
[7] E. Barberio *et al.* (Heavy Flavor Averaging Group), arXiv:0808.1297.
[8] M. Bona *et al.* (UTfit Collaboration), PMC Phys. A **3**, 6 (2009).
[9] S. Baek, C. W. Chiang, and D. London, Phys. Lett. B **675**, 59 (2009).
[10] T. Feldmann and J. Matias, J. High Energy Phys. 01 (2003) 074; B. Aubert *et al.* (*BABAR* Collaboration), Phys. Rev. Lett. **102**, 091803 (2009).
[11] K. Kiers, T. Knighton, D. London, M. Russell, A. Szynkman, and K. Webster, Phys. Rev. D **84**, 074018 (2011).
[12] G. Burdman, Phys. Rev. D **57**, 4254 (1998).
[13] A. Ali, P. Ball, L. T. Handoko, and G. Hiller, Phys. Rev. D **61**, 074024 (2000).
[14] M. Beneke, T. Feldmann, and D. Seidel, Nucl. Phys. **B612**, 25 (2001).
[15] R. Aaij (LHCb Collaboration), Phys. Rev. Lett. **108**, 181806 (2012).
[16] A. Ishikawa *et al.*, Phys. Rev. Lett. **96**, 251801 (2006).
[17] J. T. Wei *et al.* (BELLE Collaboration), Phys. Rev. Lett. **103**, 171801 (2009).
[18] B. Aubert *et al.* (*BABAR* Collaboration), Phys. Rev. D **73**, 092001 (2006).

[19] A. S. Cornell, N. Gaur, and S. K. Singh, arXiv:hep-ph/0505136.
[20] A. Ali, T. Mannel, and T. Morozumi, Phys. Lett. B **273**, 505 (1991).
[21] M. Misiak, Nucl. Phys. **B393**, 23 (1993); **B439**, 461(E) (1995).
[22] F. Kruger and E. Lunghi, Phys. Rev. D **63**, 014013 (2000).
[23] A. Ali, E. Lunghi, C. Greub, and G. Hiller, Phys. Rev. D **66**, 034002 (2002).
[24] A. Ghinculov, T. Hurth, G. Isidori, and Y. P. Yao, Eur. Phys. J. C **33**, s288 (2004).
[25] C. Bobeth, T. Ewerth, F. Kruger, and J. Urban, Phys. Rev. D **64**, 074014 (2001).
[26] P. H. Chankowski and L. Slawianowska, Eur. Phys. J. C **33**, 123 (2004).
[27] G. Hiller and F. Kruger, Phys. Rev. D **69**, 074020 (2004).
[28] A. K. Alok and S. U. Sankar, Phys. Lett. B **620**, 61 (2005).
[29] A. K. Alok, A. Dighe, and S. U. Sankar, Mod. Phys. Lett. A **25**, 1099 (2010).
[30] A. K. Alok, A. Dighe, and S. U. Sankar, Phys. Rev. D **78**, 034020 (2008).
[31] A. Hovhannisyan, W. S. Hou, and N. Mahajan, Phys. Rev. D **77**, 014016 (2008).
[32] F. Kruger and J. Matias, Phys. Rev. D **71**, 094009 (2005).
[33] E. Lunghi and J. Matias, J. High Energy Phys. 04 (2007) 058.
[34] U. Egede, T. Hurth, J. Matias, M. Ramon, and W. Reece, J. High Energy Phys. 11 (2008) 032.
[35] T. M. Aliev, V. Bashiry, and M. Savci, Eur. Phys. J. C **35**, 197 (2004).
[36] T. M. Aliev, V. Bashiry, and M. Savci, J. High Energy Phys. 05 (2004) 037.
[37] T. M. Aliev, M. K. Cakmak, A. Ozpineci, and M. Savci, Phys. Rev. D **64**, 055007 (2001).
[38] W. Bensalem, D. London, N. Sinha, and R. Sinha, Phys. Rev. D **67**, 034007 (2003).
[39] A. K. Kumar, A. Dighe, D. Ghosh, D. London, J. Matias, M. Nagashima, and A. Sznkman, J. High Energy Phys. 02 (2010) 053.
[40] T. Aaltonen *et al.* (CDF Collaboration), Phys. Rev. Lett. **106**, 161801 (2011).
[41] R. Fleischer and R. Knegjens, Eur. Phys. J. C **71**, 1789 (2011).
[42] F. Azfar *et al.* (CDF Collaboration), Public Note 10206 (2010).
[43] V. M. Abazov *et al.* (D0 Collaboration), Phys. Rev. D **85**, 032006 (2012).
[44] R. Van Kooten, in Lepton-Photon 2011, Mumbai, India, 2011, http://www.tifr.res.in/~lp11/.
[45] V. M. Abazov *et al.* (D0 Collaboration), Phys. Rev. D **84**, 052007 (2011).
[46] G. Raven, in Lepton-Photon 2011, Mumbai, India, 2011, http://www.tifr.res.in/~lp11/.
[47] U. O. Yilmaz, Eur. Phys. J. C **58**, 555 (2008).
[48] G. Erkol and G. Turan, Eur. Phys. J. C **25**, 575 (2002).
[49] Q. Chang and Y. H. Gao, Nucl. Phys. **B845**, 179 (2011).
[50] R. Mohanta and A. K. Giri, Phys. Rev. D **75**, 035008 (2007).
[51] Y. Li and J. Hua, Eur. Phys. J. C **71**, 1764 (2011).
[52] P. Ball and V. M. Braun, Phys. Rev. D **58**, 094016 (1998).
[53] P. Ball and R. Zwicky, Phys. Rev. D **71**, 014029 (2005).
[54] Y. L. Wu, M. Zhong, and Y. B. Zuo, Int. J. Mod. Phys. A **21**, 6125 (2006).
[55] W. Wang, R. H. Li, and C. D. Lu, arXiv:0711.0432.
[56] D. Melikhov and B. Stech, Phys. Rev. D **62**, 014006 (2000).
[57] A. Deandrea and A. D. Polosa, Phys. Rev. D **64**, 074012 (2001).
[58] C. Q. Geng and C. C. Liu, J. Phys. G **29**, 1103 (2003).
[59] C. M. Bouchard *et al.*, Proc. Sci., LATTICE (2012) 118.
[60] G. Buchalla, A. J. Buras, and M. E. Lautenbacher, Rev. Mod. Phys. **68**, 1125 (1996).
[61] A. J. Buras and M. Munz, Phys. Rev. D **52**, 186 (1995).
[62] C. S. Lim, T. Morozumi, and A. I. Sanda, Phys. Lett. B **218**, 343 (1989).
[63] A. Ali, T. Mannel, and T. Morozumi, Phys. Lett. B **273**, 505 (1991).
[64] F. Kruger and L. M. Sehgal, Phys. Lett. B **380**, 199 (1996).
[65] B. Grinstein, M. J. Savage, and M. B. Wise, Nucl. Phys. **B319**, 271 (1989).
[66] G. Cella, G. Ricciardi, and A. Vicere, Phys. Lett. B **258**, 212 (1991).
[67] C. Bobeth, M. Misiak, and J. Urban, Nucl. Phys. **B574**, 291 (2000).
[68] H. H. Asatrian, H. M. Asatrian, C. Greub, and M. Walker, Phys. Lett. B **507**, 162 (2001).
[69] M. Misiak, Nucl. Phys. **B393**, 23 (1993); **B439**, 461(E) (1995).
[70] D. Melikhov, N. Nikitin, and S. Simula, Phys. Lett. B **430**, 332 (1998).
[71] J. M. Soares, Nucl. Phys. **B367**, 575 (1991).
[72] G. M. Asatrian and A. Ioannisian, Phys. Rev. D **54**, 5642 (1996).
[73] J. M. Soares, Phys. Rev. D **53**, 241 (1996).
[74] C. H. Chen and C. Q. Geng, Phys. Rev. D **64**, 074001 (2001).
[75] T. Huber, T. Hurth, and E. Lunghi, arXiv:0807.1940.
[76] D. Melikhov, N. Nikitin, and S. Simula, Phys. Lett. B **430**, 332 (1998).
[77] J. M. Soares, Nucl. Phys. **B367**, 575 (1991).
[78] G. M. Asatrian and A. Ioannisian, Phys. Rev. D **54**, 5642 (1996).
[79] T. Appelquist, H. C. Cheng, and B. A. Dobrescu, Phys. Rev. D **64**, 035002 (2001).
[80] A. J. Buras, M. Spranger, and A. Weiler, Nucl. Phys. **B660**, 225 (2003).
[81] A. J. Buras, A. Poschenrieder, M. Spranger, and A. Weiler, Nucl. Phys. **B678**, 455 (2004).
[82] P. Langacker and M. Plumacher, Phys. Rev. D **62**, 013006 (2000).
[83] V. Barger, L. Everett, J. Jiang, P. Langacker, T. Liu, and C. Wagner, Phys. Rev. D **80**, 055008 (2009).
[84] M. J. Aslam, C.-D. Lu, and Y.-M. Wang, Phys. Rev. D **79**, 074007 (2009).
[85] M. J. Aslam, Y.-M. Wang, and C.-D. Lu, Phys. Rev. D **78**, 114032 (2008).
[86] T. M. Aliev and M. Savci, Eur. Phys. J. C **50**, 91 (2007).
[87] V. Bashiry and K. Azizi, J. High Energy Phys. 02 (2012) 021.

[88] P. Colangelo, F. De Fazio, R. Ferrandes, and T. Pham, Phys. Rev. D **74**, 115006 (2006); A. Siddique, M. J. Aslam, and C.-D. Lü, Eur. Phys. J. C **56**, 267 (2008).
[89] M. A. Paracha, I. Ahmed, and M. J. Aslam, Phys. Rev. D **84**, 035003 (2011).
[90] I. Ahmed, M. J. Aslam and M. A. Paracha (unpublished).
[91] U. Haisch and A. Weiler, Phys. Rev. D **76**, 034014 (2007).
[92] I. Gogoladze and C. Macesanu, Phys. Rev. D **74**, 093012 (2006).
[93] J. A. R. Cembranos, J. L. Feng, and L. E. Strigari, Phys. Rev. D **75**, 036004 (2007).
[94] V. Barger, C. W. Chiang, P. Langacker, and H. S. Lee, Phys. Lett. B **598**, 218 (2004).
[95] Q. Chang, X. Q. Li, and Y. D. Yang, J. High Energy Phys. 05 (2009) 056.
[96] V. Barger, L. Everett, J. Jiang, P. Langacker, T. Liu, and C. Wagner, Phys. Rev. D **80**, 055008 (2009).
[97] V. Barger, L. Everett, J. Jiang, P. Langacker, T. Liu, and C. Wagner, J. High Energy Phys. 12 (2009) 048.
[98] Q. Chang, X. Q. Li, and Y. D. Yang, J. High Energy Phys. 02 (2010) 082.